OPEN ACCESS Freely available online

PLOS ONE

Mouse Model for ROS1-Rearranged Lung Cancer

Yasuhito Arai[1☯], Yasushi Totoki[1☯], Hiroyuki Takahashi[1], Hiromi Nakamura[1], Natsuko Hama[1], Takashi Kohno[2], Koji Tsuta[3], Akihiko Yoshida[3], Hisao Asamura[4], Michihiro Mutoh[5], Fumie Hosoda[1], Hitoshi Tsuda[3], Tatsuhiro Shibata[1]*

1 Division of Cancer Genomics, National Cancer Center Research Institute, Chuo-ku, Tokyo, Japan, **2** Division of Genome Biology, National Cancer Center Research Institute, Chuo-ku, Tokyo, Japan, **3** Division of Pathology and Clinical Laboratories, National Cancer Center Hospital, Chuo-ku, Tokyo, Japan, **4** Thoracic Surgery Division, National Cancer Center Hospital, Chuo-ku, Tokyo, Japan, **5** Division of Cancer Prevention Research, National Cancer Center Research Institute, Chuo-ku, Tokyo, Japan

Abstract

Genetic rearrangement of the *ROS1* receptor tyrosine kinase was recently identified as a distinct molecular signature for human non-small cell lung cancer (NSCLC). However, direct evidence of lung carcinogenesis induced by *ROS1* fusion genes remains to be verified. The present study shows that *EZR-ROS1* plays an essential role in the oncogenesis of NSCLC harboring the fusion gene. *EZR-ROS1* was identified in four female patients of lung adenocarcinoma. Three of them were never smokers. Interstitial deletion of 6q22–q25 resulted in gene fusion. Expression of the fusion kinase in NIH3T3 cells induced anchorage-independent growth *in vitro*, and subcutaneous tumors in nude mice. This transforming ability was attributable to its kinase activity. The ALK/MET/ROS1 kinase inhibitor, crizotinib, suppressed fusion-induced anchorage-independent growth of NIH3T3 cells. Most importantly, established transgenic mouse lines specifically expressing EZR-ROS1 in lung alveolar epithelial cells developed multiple adenocarcinoma nodules in both lungs at an early age. These data suggest that the *EZR-ROS1* is a pivotal oncogene in human NSCLC, and that this animal model could be valuable for exploring therapeutic agents against *ROS1*-rearranged lung cancer.

Citation: Arai Y, Totoki Y, Takahashi H, Nakamura H, Hama N, et al. (2013) Mouse Model for ROS1-Rearranged Lung Cancer. PLoS ONE 8(2): e56010. doi:10.1371/journal.pone.0056010

Editor: John D. Minna, Univesity of Texas Southwestern Medical Center at Dallas, United States of America

Received October 3, 2012; **Accepted** January 4, 2013; **Published** February 13, 2013

Funding: This study was supported by the Program for Promotion of Fundamental Studies in Health Sciences from the National Institute of Biomedical Innovation, National Cancer Center Research and Development Funds (23-A-7 and 23-B-28), Research Grant of the Princess Takamatsu Cancer Research Fund and Grants-in-Aid from the Ministry of Health, Labour and Welfare for the 3rd-term Comprehensive 10-year Strategy for Cancer Control. National Cancer Center Biobank is supported by the National Cancer Center Research and Development Fund, Japan. The funders had no role in study design, data collection and analysis, decision to publish, or preparation of the manuscript.

Competing Interests: The authors have declared that no competing interests exist.

* E-mail: tashibat@ncc.go.jp

☯ These authors contributed equally to this work.

Introduction

Lung cancer is the leading cause of cancer death around the world [1]. Lung adenocarcinoma (LADC), the most common form of non-small-cell lung cancer (NSCLC), comprises several different genomic subsets defined by unique oncogenic alterations, and a considerable proportion of LADC cases harbor driver alterations in the *EGFR*, *KRAS* and *ALK* genes at the mutually exclusive manner with rare exceptions [2–5]. Understanding the molecular basis of cancer allows us to develop therapeutic agents that target genetic druggable aberrations identified in cancer genomes. Tyrosine kinase inhibitors (TKIs) that target the EGFR and ALK proteins are particularly effective in the treatment of LADC carrying *EGFR* mutations and *ALK* fusions, respectively [2-6]. However, the development of an effective TKI requires experimental validation of the genetic aberrations as actionable and druggable. Transgenic mouse models harboring *EGFR* mutations or *EML4-ALK* gene fusions have successfully demonstrated the oncogenic potential of the alterations and the efficacy of TKI therapy [7,8]. Genetic rearrangement of the *ROS1* was recently identified as a distinct molecular signature for human LADC [9-16]. In the present study, we established a mouse model of *ROS1* fusion, and showed that *EZR-ROS1* as an essential driver oncogene in lung carcinogenesis.

Results

Identification of EZR-ROS1 Fusion Gene in LADC of Never-smokers

Whole transcriptome high-throughput sequencing of tumor specimens is one of the most effective methods for identifying fusion oncogenes [17]. Analysis of five LADC cases of never-smokers without *EGFR/KRAS/ALK* alterations using transcriptome sequencing identified 56 reads overriding the in-frame *EZR-ROS1* gene fusion point connecting *EZR* exon 10 to *ROS1* exon 34 in one tumor. RT-PCR analysis of matched non-cancerous tissues confirmed tumor-specific expression of the fusion transcript (Figure 1A). In addition, transcriptome sequencing clearly demonstrated a specific increase in the expression of the fused 3′ portion of *ROS1* (exons 34 to 43) after the breakpoint, suggesting that the *EZR-ROS1* fusion transcript causes aberrant overexpression of *ROS1* tyrosine kinase domain along with the 5′ portion of *EZR* (Figure 1B). SNP array comparative genomic hybridization (array CGH) data showed that this fusion gene was generated by a large interstitial deletion spanning ~41.5 Mb on chromosome 6q22-q25 (Figure 1C). Genomic PCR and sequencing analysis also revealed the deletion of 41.5 Mb causing somatic fusions of the

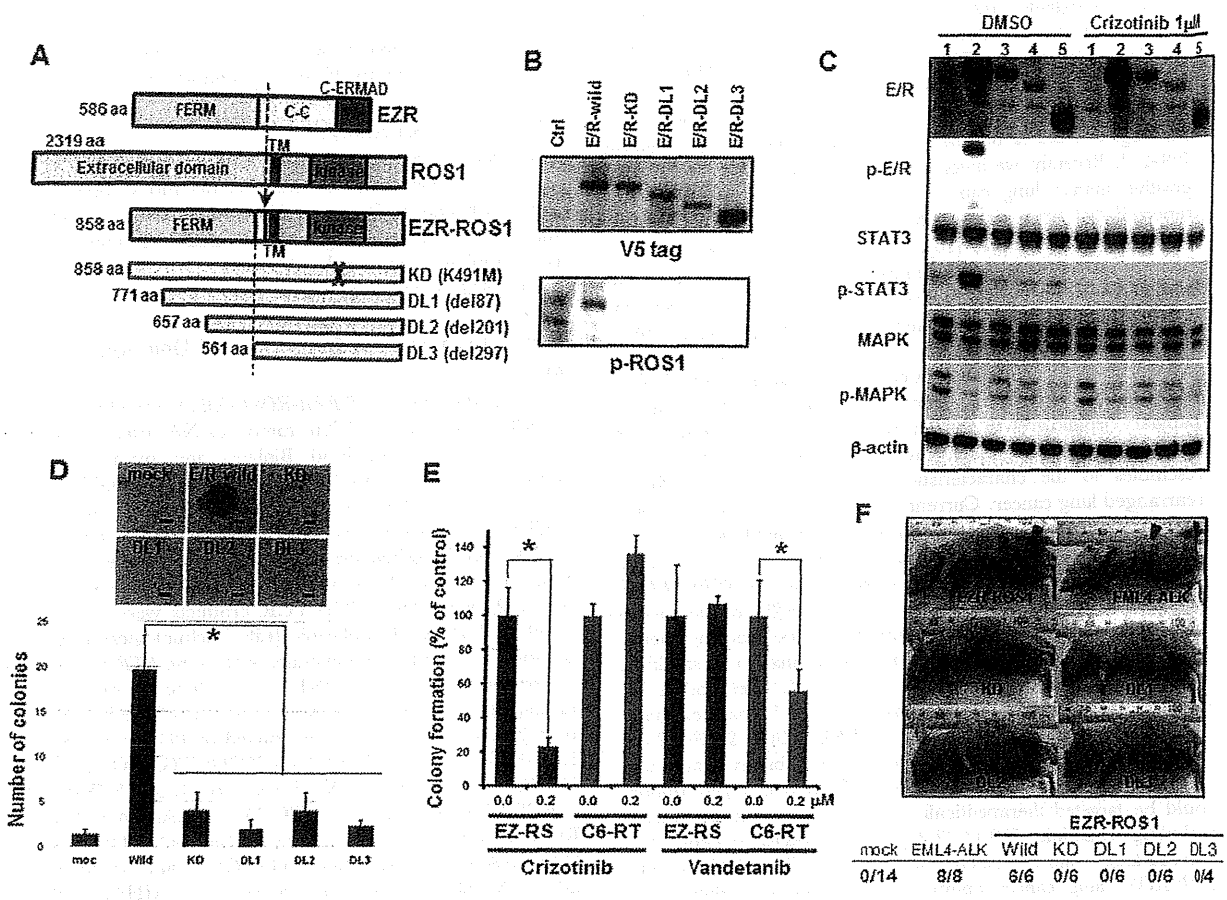

Figure 2. Oncogenic activity of the *EZR-ROS1* fusion gene. (A) Schematic representation of EZR, ROS1, EZR-ROS1, and deletions/mutations of EZR-ROS1 genes. The domain organization is shown. C-C: coiled-coil domain; TM: transmembrane; C-ERMAD: C-terminal ERM associated domain. (B) ROS1 phosphorylation in wild-type and mutant EZR-ROS1 (E/R)-expressing NIH3T3 clones. Cell lysates from each clone were immunoblotted with anti-V5-tag (top) and anti-phosphorylated ROS1 (Tyr-2274, bottom) antibodies. (C) Suppression of ROS 1 kinase activity of EZR-ROS1 by crizotinib inhibits STAT3 activation. NIH3T3 cells transfected with 1: empty vector, 2: wild-type EZR-ROS1, 3: KD 4: DL1, 5: DL3 were serum starved and treated for 2 hr with DMSO or 1 μM of crizotinib, and immunoblotted with the relevant antibodies. β-actin was used as a loading control. E/R: EZR-ROS1, p-E/R: phosphorylated EZR-ROS1 detected with an anti-phosphotyrosine-2274 antibody of ROS1. (D) Soft agar colony formation of wild-type and mutant EZR-ROS1 expressing NIH3T3 clones. A representative picture of colony formation for each clone is plotted at the top (scale bar, 100 μm). The number of colonies obtained for each clone is plotted at the bottom. *P<0.05. (E) Crizotinib-induced suppression of anchorage-independent growth of NIH3T3 cells expressing EZR-ROS1. Bar graph showing the percentage of NIH3T3 colonies induced by *EZR-ROS1* or *CCDC6-RET* after treatment with 200 nM of crizotinib or vandetanib with respect to those formed by DMSO-treated cells. EZ-ROS: EZR-ROS1, C6-RET: CCDC6-RET. *P<0.05. (F) Representative pictures of mice subcutaneously transplanted with NIH3T3 cells expressing wild-type, kinase domain-mutated, or amino-terminal-deleted EZR-ROS1. An EML4-ALK-expressing NIH3T3 clone was used as a positive control. The number of tumors per injection in each transfectant is shown below the photographs.
doi:10.1371/journal.pone.0056010.g002

and DL mutants-expressing clones produced tumors (Figure 2F), confirming that *in vivo* tumorigenic activity of *EZR-ROS1* requires ROS1 kinase activity.

Development of LADC in EZR-ROS1 Transgenic Mice

To further evaluate the role of *EZR-ROS1* in lung carcinogenesis, we generated transgenic mice expressing the fusion gene under the control of a type 2 alveolar epithelium-specific surfactant C gene promoter [20] (Figure 3A). We obtained four independent lines (TgA, B, C and D) with different copy number of the transgene (Figure S3) and detected lung adenocarcinoma nodules in all lines examined except TgD. Analysis of fusion protein expression level among them revealed no expression in TgD (Figure S4). The birth rate of transgene-positive progenies was low in TgC (Transgene-positive F1 progeny number : total F1 number; 1:3), and we failed to keep up a TgC line, then we mainly analyzed one line (TgA), which harbors approximately four copies of the transgene. RT-PCR and immunoblot analysis verified lung-specific *EZR-ROS1* mRNA and protein expression, and indicated phosphorylation of the EZR-ROS1 fusion protein (Figure 3B). Although endogenous *Ezrin* was ubiquitously expressed in many tissues, endogenous *Ros1*-transcript was detected only in stomach, kidney and lung. Protein expression levels of endogenous ROS1 were very weak compared with the levels of the fusion gene in the transgenic mice (Figure S4). Even at the four-week-old, multiple lesions over 1 mm in diameter were detected in the transgenic mice, and tumors occupied over 40% of sectioned surface of lung (Figure 3C and Figure S5). Computed tomography examination

The transgenic mice showed an emergence of multiple adenocarcinoma nodules at an early point, and the fast progression of the tumors. These features are broadly similar to the *EML4-ALK* mouse model [8]. Several groups reported that mucinous cribriform pattern and signet ring cell are characteristic histological features of *EML4-ALK* positive human lung cancer [23–25]. Recently, we investigated histopathology of *ROS1*-fusion positive human lung cancers [16]. Although other researchers reported that signet ring cell feature was not common in *ROS1*-rearranged lung cancers [10], we found that 53% of the cases harbored mucinous cribriform or signet ring cell features similar to the *ALK*-rearranged lung cancers but that the rest showed papillary/lepidic growth pattern. *EZR-ROS1*-positive tumors seemed less well differentiated, and showed more frequently histological features of mucinous cribriform or signet ring cell. Our mouse model of *EZR-ROS1* lung cancer generally demonstrated papillary/lepidic growth pattern, but in some cases, we observed accumulation of cytoplasmic mucin in tumor cells, which quite resembles to the characteristic histology reported in *ROS1*-rearranged lung cancer. Currently we have no answer why only part of mice harbored tumors with mucin accumulation.

The *EZR-ROS1* fusion gene was specifically detected in lung cancer specimens of female never-smokers without *EGFR, KRAS,* and *ALK* alterations. It was estimated that ~2% of patients in White and Asian lung cancer cohorts had *ROS1*-rearrangements, which occur at significantly higher rates in younger, non-smoking, female individuals [10,11,16]. Although each alteration is infrequent, *ROS1* fusions with many kinds of 5′ partner genes (*CCDC6, CD74, EZR, FIG, KDELR2, LRIG3, SDC4, SLC34A2 and TPM3*) have been reported in lung, brain, biliary tract, and ovarian cancers [9–16,26–28]. These *ROS1*-rearranged tumors could be targeted therapeutically with specific kinase inhibitors, including crizotinib [10,14,27,29]. Two LADC patients had a remarkable clinical response to crizotinib [10,14]. Thus, our *EZR-ROS1* lung cancer animal model could be valuable for evaluating the therapeutic potential of these compounds and novel drugs as well as biological features of *ROS1*-rearranged lung cancer *in vivo*.

Materials and Methods

Clinical Samples

Tissue specimens from lung cancer patients were provided by the National Cancer Center Biobank, Japan. High-molecular weight genomic DNA and RNA were extracted from fresh frozen tumor specimens and non-cancerous lung tissues. Written informed consent was obtained from each patient. The study protocol was approved by the Ethical Committee of National Cancer Center, Tokyo, Japan.

Analysis of Whole-transcriptome Sequence Data

Insert cDNA libraries (150–200 bp) were prepared from 2 μg of total RNA using the mRNAseq Sample Preparation Kit (Illumina). The libraries were subjected to paired-end sequencing of 50 bp on the HiSeq2000 (Illumina), according to the manufacturer's instructions. Paired-end reads were mapped to known RNA sequences in the RefSeq, Ensembl, and LincRNA databases using the Bowtie program as described previously [30].

RT-PCR, Genomic PCR and Sequencing

Total RNA was reverse-transcribed to cDNA using Superscript III (Life Technologies). cDNA or genomic DNA was subjected to PCR amplification using Ex-Taq (Takara Bio) and primers EZR-e10-CF1 (GAAAAGGAGAGAAACCGTGGAG) and ROS1-e34-CR1 (TCAGTGGGATTGTAACAACCAG). The PCR products were directly sequenced by Sanger sequencing using the BigDye terminator kit (Life Technologies).

SNP Array CGH Analysis

Chromosomal copy number for the tumors was determined using high-resolution SNP arrays (GeneChip Mapping 250K-Nsp array, Affymetrix). Genomic DNA was labeled and hybridized to the SNP arrays according to the manufacturer's instructions, and copy numbers were calculated from the hybridization signals using the CNAG program [31].

Vector Cloning, and Generation of Deletion and Point Mutants

The coding region of *EZR-ROS1* cDNA was obtained by PCR amplification from LCY66 tumor cDNA using Phusion Taq polymerase (New England Biolabs) and primers EZR-H1F1 (CACCATGCCGAAACCAATCAATGTCCGAGTT) and ROS1-H1R1 (ATCAGACCCATCTCCATATCCACTGTG). *EML4-ALK* cDNA and *CCDC6-RET* cDNA were amplified from an *EML4-ALK*-positive primary lung cancer sample (E13;A20) and from a *CCDC6-RET*-positive primary lung cancer sample (C1;R12), respectively. The PCR products were subcloned into a pcDNA3.1D-V5-His plasmid (Life Technologies). Replacement of lysine with methionine at codon 491 in the *EZR-ROS1* gene was performed using a PrimeSTAR site-directed mutagenesis kit (Takara Bio). N-terminal deletion mutants of the FERM domain of *EZR-ROS1* cDNA were constructed by PCR using the primers EZR-FERM-AF (CACCATGGTGGCTGAGGAGCTCATCCAGGACATC) and ROS1-H1R1 for DL1, EZR-FERM-BF (CACCATGATCAACTATTTCGAGATAAAAAACAAG) and ROS1-H1R1 for DL2, and EZR-FERM-CF (CACCATGACCATCGAGGTGCAGCAGATGAAGGC) and ROS1-H1R1 for DL3. The plasmids were transfected into NIH3T3 cells using Lipofectamine 2000 reagent (Life Technologies), and stable clones were isolated by G418 selection (0.7 mg/ml). For the colony formation assay, cells were embedded and cultured in 0.4% soft agar in triplicate and the number of colonies was counted after 21 days. Quantification of anchorage–independent growth under the condition with or without crizotinib (S1068, Selleck) and vandetanib (S1046, Selleck) after 9 days was performed with CytoSelect-96 kit (Cell Biolabs). The compound solution was added to the top layer of soft agar every 3 days.

Immunoblot Analysis

Whole cell lysates were extracted with CelLytic M reagent (#C2978, Sigma), and subjected to SDS-PAGE followed by blotting onto a PVDF membrane. Detection of Western blots was performed with the WesternBreeze Chemiluminescent Immunodetection kit (Life Technologies) using primary antibodies against ROS1 (#9202, Cell Signaling Technology), phosphorylated-ROS1 (Tyr2274) (#3078, Cell Signaling Technology), STAT3 (#610189, BD), phosphorylated-STAT3 (Tyr705) (#9138, Cell Signaling Technology), p44/42 MAPK (#4695, Cell Signaling Technology), phosphorylated-p44/42 MAPK (Thr202/Tyr204) (#9106, Cell Signaling Technology), Ezrin (#4135, Cell Signaling Technology), p53 (#6243, Santa Cruz), and b-actin (#A5441, Sigma).

Suppression of ROS 1 Kinase Activity of EZR-ROS1 by Crizotinib

Transfected NIH3T3 cells (empty vector, wild-type EZR-ROS1, KD/DL mutants) were serum starved for 2 hr, then

7. Li D, Shimamura T, Ji H, Chen L, Haringsma HJ, et al. (2007) Bronchial and peripheral murine lung carcinomas induced by T790M-L858R mutant EGFR respond to HKI-272 and rapamycin combination therapy. Cancer Cell 12: 81–93.
8. Soda M, Takada S, Takeuchi K, Choi YL, Enomoto M, et al. (2008) A mouse model for EML4-ALK-positive lung cancer. Proc Natl Acad Sci U S A 105: 19893–19897.
9. Rikova K, Guo A, Zeng Q, Possemato A, Yu J, et al. (2007) Global survey of phosphotyrosine signaling identifies oncogenic kinases in lung cancer. Cell 131: 1190–1203.
10. Bergethon K, Shaw AT, Ou SH, Katayama R, Lovly CM, et al. (2012) ROS1 Rearrangements define a unique molecular class of lung cancers. J Clin Oncol 30: 863–870.
11. Takeuchi K, Soda M, Togashi Y, Suzuki R, Sakata S, et al. (2012) RET, ROS1 and ALK fusions in lung cancer. Nat Med. 18: 378–381.
12. Rimkunas VM, Crosby KE, Li D, Hu Y, Kelly ME, et al. (2012) Analysis of Receptor Tyrosine Kinase ROS1-Positive Tumors in Non-Small Cell Lung Cancer: Identification of a FIG-ROS1 Fusion. Clin Cancer Res 18: 4449–4457.
13. Seo JS, Ju YS, Lee WC, Shin JY, Lee JK, et al. (2012) The transcriptional landscape and mutational profile of lung adenocarcinoma. Genome Res 22: 2109–2119.
14. Davies KD, Le AT, Theodoro MF, Skokan MC, Aisner DL, et al. (2012) Identifying and Targeting ROS1 Gene Fusions in Non-Small Cell Lung Cancer. Clin Cancer Res 18: 4570–4579.
15. Govindan R, Ding L, Griffith M, Subramanian J, Dees ND, et al. (2012) Genomic landscape of non-small cell lung cancer in smokers and never-smokers. Cell 150: 1121–1134.
16. Yoshida A, Kohno T, Tsuta K, Wakai S, Arai Y, et al. (in press) ROS1-rearranged lung cancer: a clinicopathological and molecular study of 15 surgical cases. Am J Surg Path in press.
17. Maher CA, Kumar-Sinha C, Cao X, Kalyana-Sundaram S, Han B, et al. (2009) Transcriptome sequencing to detect gene fusions in cancer. Nature 458: 97–101.
18. Chishti AH, Kim AC, Marfatia SM, Lutchman M, Hanspal M, et al. (1998) The FERM domain: a unique module involved in the linkage of cytoplasmic proteins to the membrane. Trends Biochem Sci 23: 281–282.
19. Charest A, Kheifets V, Park J, Lane K, McMahon K, et al. (2003) Oncogenic targeting of an activated tyrosine kinase to the Golgi apparatus in a glioblastoma. Proc Natl Acad Sci U S A. 100: 916–921.
20. Mishra A, Weaver TE, Beck DC, Rothenberg ME (2001) Interleukin-5-mediated allergic airway inflammation inhibits the human surfactant protein C promoter in transgenic mice. J Biol Chem 276: 8453–8459.
21. Fehon RG, McClatchey AI, Bretscher A (2010) Organizing the cell cortex: the role of ERM proteins. Nat Rev Mol Cell Biol 11: 276–287.
22. Medves S, Demoulin JB (2012) Tyrosine kinase gene fusions in cancer: translating mechanisms into targeted therapies. J Cell Mol Med 16: 237–248.
23. Inamura K, Takeuchi K, Togashi Y, Hatano S, Ninomiya H, et al. (2009) EML4-ALK lung cancers are characterized by rare other mutations, a TTF-1 cell lineage, an acinar histology, and young onset. Mod Pathol 22: 508–515.
24. Mino-Kenudson M, Chirieac LR, Law K, Hornick JL, Lindeman N, et al. (2010) A novel, highly sensitive antibody allows for the routine detection of ALK-rearranged lung adenocarcinomas by standard immunohistochemistry. Clin Cancer Res 16: 1561–1571.
25. Yoshida A, Tsuta K, Nakamura H, Kohno T, Takahashi F, et al. (2011) Comprehensive histologic analysis of ALK-rearranged lung carcinomas. Am J Surg Pathol 35: 1226–1234.
26. Charest A, Lane K, McMahon K, Park J, Preisinger E, et al. (2003) Fusion of FIG to the receptor tyrosine kinase ROS in a glioblastoma with an interstitial del(6)(q21q21). Genes Chromosomes Cancer 37: 58–71.
27. Gu TL, Deng X, Huang F, Tucker M, Crosby K, et al. (2011) Survey of tyrosine kinase signaling reveals ROS kinase fusions in human cholangiocarcinoma. PLoS One 6: e15640.
28. Birch AH, Arcand SL, Oros KK, Rahimi K, Watters AK, et al. (2011) Chromosome 3 anomalies investigated by genome wide SNP analysis of benign, low malignant potential and low grade ovarian serous tumours. PLoS One 6: e28250.
29. Park BS, El-Deeb IM, Yoo KH, Oh CH, Cho SJ, et al. (2009) Design, synthesis and biological evaluation of new potent and highly selective ROS1-tyrosine kinase inhibitor. Bioorg Med Chem Lett 19: 4720–4723.
30. Totoki Y, Tatsuno K, Yamamoto S, Arai Y, Hosoda F, et al. (2011) High-resolution characterization of a hepatocellular carcinoma genome. Nat Genet 43: 464–469.
31. Nannya Y, Sanada M, Nakazaki K, Hosoya N, Wang L, et al. (2005) A robust algorithm for copy number detection using high-density oligonucleotide single nucleotide polymorphism genotyping arrays. Cancer Res 65: 6071–6079.
32. Yoshikawa D, Ojima H, Kokubu A, Ochiya T, Kasai S, et al. (2009) Vandetanib (ZD6474), an inhibitor of VEGFR and EGFR signaling, as a novel molecular-targeted therapy against cholangiocarcinoma. Br J Cancer 100: 1257–1266.

Suppression of intestinal polyp development in *Apc*$^{Min/+}$ mice through inhibition of P-glycoprotein using verapamil

Kyoko Fujimoto[a], Gen Fujii[b], Michihiro Mutoh[b], Masa Yasunaga[c], Hiromitsu Tanaka[a] and Morimasa Wada[c]

P-glycoprotein (P-gp; encoded by the *Mdr1a* gene) is known to be associated with colon tumorigenesis through transcriptional activation and/or epigenetic modification. We investigated whether inhibition of P-gp function might decrease intestinal tumorigenesis. We used verapamil as an inhibitor of P-gp function in *Apc*$^{Min/+}$ mice, which lack a functional *Apc* gene product. We determined the number of intestinal polyps and 1-year survival rates after the ingestion of 10, 25, and 50 mg/kg/day verapamil contained in dry pellets. The number of polyps in *Mdr1a*$^{+/+}$*Apc*$^{Min/+}$ mice fed with pellets containing verapamil was significantly lower than that in mice fed with verapamil-free pellets. The 1-year survival rate of verapamil-fed mice was also improved in a dose-dependent manner. These results were similar to data from P-gp knockout mice. These results indicated that it might be possible to use verapamil to inhibit polyp development during the early stage of colon carcinogenesis. Thus, we propose a novel chemopreventive agent for colorectal cancer that acts by inhibiting P-gp function. *European Journal of Cancer Prevention* 22:8-10 © 2012 Wolters Kluwer Health | Lippincott Williams & Wilkins.

European Journal of Cancer Prevention 2013, 22:8–10

Keywords: chemoprevention, colorectal cancer, Mdr1a protein, verapamil

[a]Division of Molecular Biology, Nagasaki International University, Nagasaki, [b]Division of Cancer Prevention Research, National Cancer Center Research Institute, Tokyo and [c]Division of Medical Biochemistry, Kyushu University, Fukuoka, Japan

Correspondence to Morimasa Wada, PhD, Division of Molecular Biology, Nagasaki International University, 2825-7, Huis Ten Bosch, Sasebo, Nagasaki 859 3298, Japan
Tel: +81 956 20 5739; fax: +81 956 20 5649; e-mail: wadam@niu.ac.jp

Received 22 December 2011 Accepted 17 March 2012

Introduction

P-glycoprotein (P-gp) is encoded by the *Mdr1a* gene and is expressed in many tissues including the small and large intestine, hepatobiliary tract, and placenta. P-gp belongs to the ATP-binding cassette B subfamily and has a major role in the efflux of xenobiotics as a self-defense mechanism (Tanigawara, 2000). This efflux system is known to be a cause of multidrug resistance, which decreases the effects of drug treatments.

We previously demonstrated that P-gp increased the incidence of intestinal polyp development by the direct involvement of TCF/LEF transcription factor activation (Yamada *et al.*, 2003) and/or epigenetic modification (Mochida *et al.*, 2003). Therefore, we hypothesized that it may be possible to control intestinal polyp development by inhibiting P-gp function.

Verapamil has been widely used in the treatment of ischemic heart disease since the 1960s (Haas and Igarashi, 1968). This agent is characterized by intestinal absorption, and it is also a substrate of P-gp. Numerous studies have demonstrated that verapamil can inhibit the efficiency of the efflux function of P-gp through an antagonistic action (Cornwell *et al.*, 1987; Qian and Beck, 1990).

In this study, we examined whether inhibition of P-gp function using verapamil or P-gp deficiency would decrease the number of intestinal polyps that developed in mice lacking a functional *Apc* gene product (*Apc*$^{Min/+}$), which is a model of human familial adenomatous polyposis.

Methods

Mice

The *Mdr1a* knockout mice (FVB/N) were obtained from Taconic Farms (Germantown, New York, USA), whereas the *Apc*$^{Min/+}$ (C57B1/6J) mice were supplied by Jackson Laboratories (Bar Harbor, Maine, USA). The mice were maintained under specific pathogen-free conditions at the Center of Biomedical Research, Kyushu University (Fukuoka, Japan). Generation of *Mdr1a*$^{-/-}$*Apc*$^{Min/+}$ mice is described elsewhere (Mochida *et al.*, 2003).

We analyzed 14 mice, which were fed a verapamil-free diet; and 15 mice, which were fed with verapamil. Mice were killed at 5–12 months of age for the analysis of intestinal polyps. All animal experiments were carried out according to the Guidelines for Animal Experiments in the Faculty of Medical Sciences, Kyushu University.

Feed

The mouse feed was compounded with three different doses of verapamil (Vasolan; Eisai, Japan), that is 10, 25, and 50 mg/kg/day. In addition, a verapamil-free control group was also maintained. According to the data sheet provided by the company (Eisai), the maximum acceptable dose of verapamil for an adult dog is 25 mg/kg/day. On the basis of this, we calculated the appropriate dose for mice.

0959-8278 © 2012 Wolters Kluwer Health | Lippincott Williams & Wilkins

DOI: 10.1097/CEJ.0b013e32835ede8

Table 1 The number of intestinal polyps in each mouse

Mouse strain	Dosage of verapamil (mg/kg/day)	Small intestine			Small intestine	Large intestine	Total
		Distal	Middle	Proximal			
Mdr1a$^{+/+}$*Apc*$^{Min/+}$	0	39.8±5.1	20.4±4.3	6.0±1.5	66.4±9.8	3.0±0.8	69.2±9.7
	10	16.2±2.5*	7.4±1.4*	3.3±0.8	26.8±3.9*	1.6±0.6	28.4±4.2*
	25	15.5±2.1*	8.5±1.5*	3.2±0.8	27.1±3.3*	2.2±0.5	29.3±3.3*
	50	14.2±2.0*	6.9±1.1*	3.2±0.8	24.3±3.3*	2.9±0.7	27.2±3.3*
Mdr1a$^{-/-}$*Apc*$^{Min/+}$	0	11.2±2.7*	4.4±1.1*	2.1±0.6	17.8±4.0*	1.6±0.6	19.4±4.4*

Values are mean±SEM.
*P<0.001 Dunnett's multiple comparison test.

Fig. 1

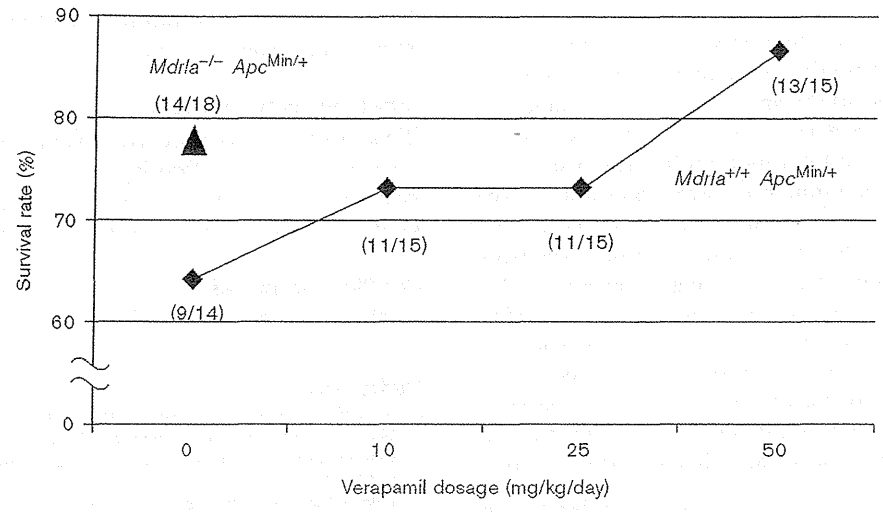

One-year survival rates of *Mdr1a*$^{+/+}$*Apc*$^{Min/+}$ (♦) and *Mdr1a*$^{-/-}$*Apc*$^{Min/+}$ mice (▲). The number of mice that survived for 1 year and the original number of mice are given in parentheses.

Genotyping

Genotyping was carried out for each mouse tail sample using a Genomic DNA Purification Kit (Qiagen, Germany), according to the manufacturer's protocol. Allele-specific PCR primers for the *Apc* and *Mdr1a* genes were produced according to previously published methods (Mochida *et al.*, 2003).

Counts of intestinal polyps and statistical analysis

Intestinal polyps were counted according to previously published methods (Mochida *et al.*, 2003). All statistical analyses were carried out using the GraphPad Prism5 program (GraphPad Software Inc., San Diego, California, USA). The correlations of the number of polyps in the mice that ate pellets with and without verapamil and P-gp knockout mice were tested using Dunnett's method. Survival rates were calculated by dividing the number of mice that survived for 1 year by the original number of mice.

Results

Inhibition of P-glycoprotein function using verapamil decreased the number of intestinal polyps

The number of intestinal polyps in *Mdr1a*$^{+/+}$*Apc*$^{Min/+}$ mice that survived for 1 year is shown in Table 1. The mean number of polyps in the small intestines of *Mdr1a*$^{+/+}$*Apc*$^{Min/+}$ mice that were fed pellets containing 10, 25, and 50 mg/kg/day verapamil was significantly lower, that is 26.8, 27.1, and 24.3, respectively, than that in mice fed with verapamil-free diet, which had a mean polyp count of 66.4. In the distal and middle parts of the small intestine, the mean number of polyps was decreased in a dose-dependent manner ($P < 0.001$).

We also crossed *Mdr1a*$^{-/-}$ mice with *Apc*$^{Min/+}$ mice to generate *Mdr1a*$^{-/-}$*Apc*$^{Min/+}$ mice and tested whether verapamil had similar effects on intestinal polyp development as in mice lacking P-gp. We compared the number of intestinal polyps in the *Mdr1a*$^{+/+}$*Apc*$^{Min/+}$ mice treated with verapamil with the P-gp knockout mice (*Mdr1a*$^{-/-}$*Apc*$^{Min/+}$). The number of polyps in *Mdr1a*$^{+/+}$*Apc*$^{Min/+}$ mice with 50 mg/kg/day verapamil was similar to that in *Mdr1a*$^{-/-}$*Apc*$^{Min/+}$ mice (Table 1).

Survival benefits of inhibiting P-glycoprotein function with verapamil

A major cause of lower survival rates in *Apc*$^{Min/+}$ mice is the development of intestinal polyps with bleeding. Thus, we

calculated the 1-year survival rates of *Mdr1a*$^{+/+}$*Apc*$^{Min/+}$ mice, which were treated with or without verapamil (Fig. 1). The survival rate of control mice fed with verapamil-free pellets was the lowest (9/14; 64.3%). Mice began to die from the age of 5 months. The survival rates of the verapamil-fed groups increased in a dose-dependent manner as follows: 11/15 (73.3%) with 10 mg/kg/day, 11/15 (73.3%) with 25 mg/kg/day, and 13/15 (86.7%) with 50 mg/kg/day verapamil. The survival rate of *Mdr1a*$^{+/+}$*Apc*$^{Min/+}$ mice fed with 50 mg/kg/day verapamil was higher than that of *Mdr1a*$^{-/-}$*Apc*$^{Min/+}$ mice (14/18; 77.8%).

Discussion

Chemoprevention is a strong strategy to overcome colorectal cancer, but it is still a challenging issue (Herszenyi *et al.*, 2008). This study showed that the number of intestinal polyps in *Mdr1a*$^{+/+}$*Apc*$^{Min/+}$ mice was significantly decreased by inhibiting P-gp function using verapamil (Table 1). The number of polyps was similar to that found in *Mdr1a*$^{-/-}$*Apc*$^{Min/+}$ mice; hence, we considered that the inhibition of P-gp function using verapamil produced the same effects as P-gp knockout. The maximum effect was observed in the distal and middle parts of the small intestine because the majority of verapamil absorption occurred in these parts. The greater effectiveness in the distal and middle parts of the small intestine may also be attributable to differences in contact duration with the verapamil-supplemented diet.

To check that there was no quantitative difference in P-gp expression between the control and verapamil-fed groups, we analyzed P-gp expression in the small intestine by immunohistochemical staining. We detected no compensatory feedback increase in P-gp expression, regardless of the verapamil intake (data not shown).

Furthermore, we found that the 1-year survival rates of *Mdr1a*$^{+/+}$*Apc*$^{Min/+}$ mice fed with pellets containing verapamil were improved in a verapamil dose-dependent manner (Fig. 1). Verapamil has been used as an inhibitor of P-gp function (Fujimoto *et al.*, 2009; Munić *et al.*, 2010) and it might be effective for prolonging the lifespan, because the survival rates of mice fed with 50 mg/kg/day verapamil tended to be higher than those of *Mdr1a*$^{-/-}$*Apc*$^{Min/+}$ mice. In addition to reducing small intestinal polyp formation, the effects of verapamil on lifespan elongation should be examined in the near future.

We demonstrated that the inhibition of P-gp function led to improved survival rates and lower intestinal tumorigenesis in mice. The inhibition of P-gp function had similar effects to a defective P-gp gene. Verapamil is a medicine that has already been widely used in humans. This will make it easier to use this candidate cancer chemopreventive agent in humans. In addition, there have been no reports of specific side effects after long-term treatment with verapamil in patients with hypertension or atherosclerosis. We believe that a cancer chemopreventive agent should first be applied in a high-risk cancer group, rather than the general population. In this study, we provided evidence that verapamil was effective in a mouse model of familial adenomatous polyposis. We, then, propose that inhibiting P-gp function using verapamil could be a potent method for preventing colorectal cancer.

Acknowledgements

This study was funded by a Grant-in-Aid for Scientific Research on (C), Priority Areas (B) and Challenging Exploratory Research from the Ministry of Education, Culture, Sports, Science and Technology of Japan.

Conflicts of interest

There are no conflicts of interest.

References

Cornwell MM, Pastan I, Gottesman MM (1987). Certain calcium channel blockers bind specifically to multidrug-resistant human KB carcinoma membrane vesicles and inhibit drug binding to P-glycoprotein. *J Biol Chem* **262**: 2166–2170.

Fujimoto H, Higuchi M, Watanabe H, Koh Y, Ghosh AK, Mitsuya H, *et al.* (2009). P-glycoprotein mediates efflux transport of darunavir in human intestinal Caco-2 and ABCB1 gene-transfected renal LLC-PK1 cell lines. *Biol Pharm Bull* **32**:1588–1593.

Haas H, Igarashi T (1968). Comparative studies in the heart-lung-preparation of dog on the action spectrum of verapamil, quinidine and some alpha- and beta-sympatholytics as well as the effect of adrenaline. *Arzneimittelforschung* **18**:1373–1380.

Herszenyi L, Farinati F, Miheller P, Tulassay Z (2008). Chemoprevention of colorectal cancer: feasibility in everyday practice? *Eur J Cancer Prev* **17**:502–514.

Mochida Y, Taguchi K, Taniguchi S, Tsuneyoshi M, Kuwano H, Tsuzuki T, *et al.* (2003). The role of P-glycoprotein in intestinal tumorigenesis: disruption of *mdr1a* suppresses polyp formation in *Apc*$^{Min/+}$ mice. *Carcinogenesis* **24**:1219–1224.

Munić V, Kelnerić Z, Mikac L, Haber EV (2010). Differences in assessment of macrolide interaction with human MDR1 (ABCB1, P-gp) using rhodamine-123 efflux, ATPase activity and cellular accumulation assays. *Eur J Pharm Sci* **41**:86–95.

Qian XD, Beck WT (1990). Binding of an optically pure photoaffinity analogue of verapamil, LU-49888, to P-glycoprotein from multidrug-resistant human leukemic cell lines. *Cancer Res* **50**:1132–1137.

Tanigawara Y (2000). Role of P-glycoprotein in drug disposition. *Ther Drug Monit* **22**:137–140.

Yamada T, Mori Y, Hayashi R, Takada M, Ino Y, Naishiro Y, *et al.* (2003). Suppression of intestinal polyposis in *Mdr1*-deficient *Apc*$^{Min/+}$ mice. *Cancer Res* **63**:895–901.

Effects of Dietary Calcium on *Helicobacter pylori*-induced Gastritis in Mongolian Gerbils

MASAKI IIMURO[1], SHIRO NAKAMURA[1], TETSUO ARAKAWA[2], KEIJI WAKABAYASHI[3] and MICHIHIRO MUTOH[4]

[1]*Department of Lower Gastroenterology, Hyogo College of Medicine, Hyogo, Japan;*
[2]*Department of Gastroenterology, Graduate School of Medicine, Osaka City University, Osaka, Japan;*
[3]*Institute for Environmental Sciences, University of Shizuoka, Shizuoka, Japan;*
[4]*Division of Cancer Prevention Research, National Cancer Center Research Institute, Tokyo, Japan*

Abstract. *Background and Aims: Helicobacter pylori (Hp) infection causes gastritis and is considered a gastric cancer risk factor. We have previously reported that codfish meal markedly enhanced Hp-induced gastritis in Mongolian gerbils. In the present study, we sought the responsible components in codfish meal. Materials and Methods: Codfish were divided into three parts (meat, viscera and 'other parts', including bone), and administered to Hp-infected gerbils. Subsequently, cod bone, sardine bone and prawn shell were tested, along with major calcium components, hydroxyapatite and calcium carbonate, in bone and shell, respectively. Results: 'Other parts' and cod bone enhanced Hp-induced gastritis, as was observed for whole codfish. Similarly, sardine bone and prawn shell, as well as 0.22-0.88% hydroxyapatite and calcium carbonate, enhanced gastritis. In contrast, administration of a higher dose of the calcium compounds exerted protective effects. Conclusion: Intake of calcium compounds may contribute to enhancement of Hp-induced gastritis.*

Gastric cancer continues to be one of the most common malignancies in Japan and many other countries. Gastiric cancer risk is known to be associated with *Helicobacter pylori* (*Hp*) infection, a high intake of salty foods and an insufficient intake of fresh fruits and vegetables (1). Since half of the world's population is believed to be infected with *Hp* (2), control of *Hp*-induced disorders may lead to prevention of gastric cancer development (3-5).

Correspondence to: Michihiro Mutoh, Division of Cancer Prevention Research, National Cancer Center Research Institute, 1-1, Tsukiji 5-chome, Chuo-ku, Tokyo 104-0045, Japan. Tel: +81 335422511 ext 4351, Fax: +81 335439305, e-mail: mimutoh@ncc.go.jp

Key Words: Gastritis, *Helicobacter pylori*, fish meal, calcium, Mongolian gerbils.

Mongolian gerbils (*Meriones unguiculatus*) can readily be colonized by *Hp*, subsequently demonstrating chronic gastritis, gastric ulcers and intestinal metaplasia (6, 7). Moreover, it has been reported that *Hp* infection plus treatment with chemical carcinogens, *N*-methyl-*N*-nitrosourea (MNU) or *N*-methyl-*N'*-nitro-*N*-nitrosoguanidine, can induce gastric cancer in Mongolian gerbils, with pathological changes similar to those observed in humans (8-10). Additional treatment with 2.5-10% sodium chloride in the diet has been also reported to enhance gastric carcinogenesis in *Hp*-infected and MNU-treated Mongolian gerbils (11). Recently, a combination of 1-nitrosoindole-3-acetonitrile administration and *Hp* infection was shown to cause gastric cancer in Mongolian gerbils (12).

By using Mongolian gerbils, we have provided evidence that fish meal in conventional diets notably enhances *Hp*-induced gastritis as compared to a diet without fish meal, without any apparent major effect on numbers of *Hp* (13). However, fish meal has not yet been reported as being a risk factor for gastritis and gastric cancer. Of note, in the previous study, almost the same numbers of *Hp* were cultured from the gastric mucosa in both dietary groups (13). It has been suggested that *Hp*-induced gastritis and ulceration are influenced by both the *Hp* strain and host defensive factors. Furthermore, the potential for host defense may be affected by dietary habits (14, 15). However, risk factors regarding dietary habits for gastritis are not fully-understood, except for the case of high intake of salty foods. Thus, it is important to elucidate the components in fish meal that enhance *Hp*-induced gastritis and may thus be linked to *Hp*-related gastric carcinogenesis. Therefore, in the present study, we explored the effects of different components of fish meal and demonstrated that calcium intake in fish meal can affect *Hp*-induced gastritis in Mongolian gerbils.

Materials and Methods

Animals and chemicals. Six-week-old, specific pathogen-free male Mongolian gerbils were purchased from Seac Yoshitomi, Ltd.

(Fukuoka, Japan), and housed in polycarbonate cages on wood chip bedding in an air-conditioned biohazard room with a 12-h light/dark cycle. They were given a basal diet and water *ad libitum* until the start of the experiment. We purchased the ingredients for the conventional diet and AIN-76A from Nippon Formula Feed Manufacturing Co., Ltd. (Tokyo, Japan). Hydroxyapatite, calcium carbonate and calcium hydrogenphosphate dihydrate were purchased from Wako Pure Chemical Industries, Ltd. (Osaka, Japan). Raw codfish, sardine and prawn were purchased at Tsukiji Market (Tokyo, Japan), divided, sterilized and freeze-dried.

Preparation of test diets. The basal diet, namely 10% casein diet, was made by replacing fish meal with casein in the conventional diet containing 10% fish meal, as previously reported (13). For preparing test samples, raw codfish was divided into three parts namely meat, viscera, and other parts, including bone, and each part was sterilized, freeze-dried and cut into small pieces. The ratio of weight of meat:viscera:other was 52:3:45, respectively. These three parts were mixed with casein diet to make 5.2% meat with 4.8% casein diet, 0.3% viscera with 9.7% casein diet, and 4.5% other with 5.5% casein diet, according to the freeze-dried weight ratios. Cod bone was isolated from codfish and washed with distilled water, sterilized, freeze-dried and cut into small pieces. It was also mixed with casein diet to make a 2% test diet, because the 'other' diet contained 2% bone in freeze-dried weight. Similarly, small pieces of sardine bone and prawn shell were each blended with casein diet to make 2% test diets. We also prepared a mixture of ingredients of AIN-76A without calcium hydrogenphosphate dihydrate to make a calcium-free basal diet, designated as calcium-free AIN-76A. Hydroxyapatite, calcium carbonate and hydrogenphosphate dihydrate were each blended with this calcium-free AIN-76A to make hydroxyapatite, calcium carbonate and hydrogenphosphate dihydrate diets at concentrations of 0.22, 0.44, 0.88, 1.75 and 3.50%. These two-fold serial doses were used because 1.75% calcium hydrogenphosphate dihydrate is included in the AIN-76A diet.

H. pylori preparation. *Hp* (ATCC 43504; American Type Culture Collection, Rockville, MD, USA) bacteria were grown in brucella broth (BBL, Cockeysville, MD, USA) containing 10% heat-inactivated horse serum (Nacalai Tesque, Kyoto, Japan) for 24 h at 37°C under microaerobic conditions (5% O_2, 10% CO_2, and 85% N_2) on a rotary shaker at 120 rpm, and aliquots (4.0×10^8 CFU/ml) were used as the inoculum for the animal experiments.

Animal experimental design. Seven-week-old Mongolian gerbils were given an intragastric inoculation of the broth culture of *Hp* (0.5 ml, 2.0×10^8 CFU) after fasting for 24 h. As a control group for *Hp* infection, *Hp*-free animals received only sterilized brucella broth instead. Four hours later, all animals were fed *ad libitum* until the end of the experiment. Body weights and diet intakes were measured weekly and the general health of the animals was monitored daily.

After six weeks administration of the test diets, all animals were sacrificed under ether anesthesia at 13 weeks of age. Their stomachs were excised and opened along the greater curvature, and the contents were gently removed by washing with 10 mM phosphate buffered saline (PBS, pH 7.4). Macroscopic gastric lesions, including mucosal thickening and hemorrhage were recorded, and wet weights of the whole stomach, including the forestomach and glandular stomach, were measured. To evaluate the degree of gastric hemorrhage, the number of hemorrhagic spots was counted. Each stomach was divided into two halves, one for histological examination being fixed in 10% neutral buffered formalin, processed for embedding in paraffin and stained with hematoxylin and eosin (H&E). Determination of serum calcium and gastrin levels was performed by radioimmunoassay (RIA) and the arsenazo III method, respectively. Animal studies were performed according to the guidelines for animal experiments at the National Cancer Center.

Culture of Hp. For detection of Hp, mucosal samples of glandular stomach parts were scraped from the remaining stomach halves, homogenized with 0.3 ml PBS and diluted with the same solution. Aliquots (100 μl) of this suspension were inoculated onto segregating agar plates for *Hp* (Nissui Pharmaceutical Co., Ltd., Tokyo, Japan) with incubation at 37°C for five days under microaerobic conditions. Bacterial colonies were identified by the rapid urease test (CLO test; Tri-Med Specialties, Inc., Lenexa, KS, USA) and Gram staining for morphology. Their numbers were then counted.

Statistical analysis. All data were expressed as means±SD. Differences in incidences of gastric lesions between groups were examined for statistical significance using the Fisher's exact test, and those for other data were examined using Welch's *t*-test. $p<0.05$ was considered to be significant.

Results

Whole codfish were divided into three parts (meat, viscera and 'other parts' including fish bone) in order to examine the components responsible for enhancing gastritis in Mongolian gerbils. Administration of each part of the codfish diet did not affect the feeding or other behavior of Mongolian gerbils. No significant differences in body weight were observed among the groups.

In Table I, data for the effects of whole codfish, and the three divided fractions on *Hp*-induced gastric lesions are summarized. In the *Hp*-inoculated group fed whole codfish diet, edematous thickening was observed in the gastric mucosa, especially in the pylorus, in 7 out of 10 animals and hemorrhagic spots in 5 (Figure 1). No visible gastric lesions were observed in the basal control, codfish-meat and viscera-diet groups. On the other hand, in the 'other parts' diet group, enhancing effects similar to those observed in the group fed whole-codfish diet were noted, with edematous thickening being observed in 8 out of 10 animals and hemorrhagic spots in 9 (Figure 1). Along with edema and hemorrhage, both stomach wet weights and the number of hemorrhagic spots per animal increased significantly in groups fed whole codfish and 'other parts' diet, histological examination revealing mononuclear cell and neutrophil infiltration into the submucosal and *lamina propria* layers, and hyperplastic and cystic changes of the glandular epithelium in the pyloric region. *Hp* from all animals was successfully cultured in the all *Hp*-inoculated groups. Average numbers of viable bacteria [log (CFU/stomach)]

Table I. *Fractions of codfish and their effects on H. pylori-induced gastritis in Mongolian gerbils.*

Diet	No. of animals (%) with			No. of colonies of *H. pylori* (log CFUs/ stomach)[a]	Stomach wet weight (g)[a]	No. of hemorrhagic spots/animal[a]	Calcium levels in serum (mg/dl)[a]	Gastrin levels in serum (pg/ml)[a]
	Edema	Hemorrhage	*H. pylori* infection					
Basal	0/10 (0)	0/10 (0)	10/10 (100)	4.2±0.3	0.63±0.04	0	9.2±0.4	220±60
10% Whole codfish	7/10 (70)[b]	5/10 (50)[c]	10/10 (100)	4.1±0.7	0.93±0.24[d]	11.3±12.4[d]	9.3±0.2	320±35
5.2% Meat	0/10 (0)	0/10 (0)	10/10 (100)	4.0±0.2	0.65±0.04	0	9.1±0.4	250±72
0.3% Viscera	0/10 (0)	0/10 (0)	10/10 (100)	4.0±0.3	0.67±0.05[e]	0	9.5±0.3	260±64
4.5% Other parts	8/10 (80)[b]	9/10 (90)[b]	10/10 (100)	3.8±0.9	1.02±0.23[d]	11.9±8.1[d]	9.6±0.3	280±110

Samples were supplemented to basal (fish meal-free) diet. To evaluate the degree of gastric hemorrhage, the number of hemorrhagic spots were counted. [a]Mean±SD. [b]$p<0.01$ and [c]$p<0.05$ *versus* basal diet group by Fisher's exact test; [d]$p<0.01$ and [e]$p<0.05$ *versus* basal diet group by Welch's *t*-test.

Table II. *Effects of fish bones and prawn shell on H. pylori-induced gastritis in Mongolian gerbils.*

Diet	No. of animals (%) with			No. of colonies of *H. pylori* (log CFUs/ stomach)[a]	Stomach wet weight (g)[a]	No. of hemorrhagic spots/animal[a]
	Edema	Hemorrhage	*H. pylori* infection			
Basal	0/10 (0)	2/10 (20)	10/10 (100)	4.5±0.5	0.63±0.06	1.5±3.4
2% Cod bone	9/10 (90)[b]	8/10 (80)[c]	10/10 (100)	4.8±0.7	0.88±0.26[d]	11.7±15.3[e]
2% Sardine bone	6/10 (60)[c]	6/10 (60)	10/10 (100)	4.5±0.7	0.76±0.12[d]	7.8±7.6[e]
2% Prawn shell	7/10 (70)[b]	5/10 (50)	10/10 (100)	5.4±0.5[e]	0.84±0.26[e]	10.8±14.2[e]

Samples were supplemented to basal (fish meal-free) diet. [a]Mean±SD. [b]$p<0.01$ and [c]$p<0.05$ *versus* basal diet group by Fisher's exact test; [d]$p<0.01$ and [e]$p<0.05$ *versus* basal diet group by Welch's *t*-test.

obtained from *Hp*-infected stomach samples are also shown in Table I. No significant differences were observed among the five groups. In the *Hp*-free groups of gerbils, no gastric lesions were detected macroscopically or microscopically. Serum calcium levels ranged between 9.1-9.6 mg/dl and did not change remarkably. Serum gastrin levels tended to be higher in whole codfish and 'other parts' diet-treated animals, but not significantly.

The 'other parts' is diet mainly consisting of cod bone. Therefore, the effect of cod bone on *Hp*-induced gastritis was examined. Administration of a cod bone diet did not affect the feeding or other behavior of the gerbils. No significant differences in body weights were observed compared with the basal control group. Enhancing effects of cod bone diet on *Hp*-induced gastritis were found, as evident in Table II. The number of animals with edema, the stomach wet weights and the number of hemorrhagic spots per animal were increased significantly. No gastric lesions were detected in *Hp*-free gerbils fed the same diet. Histological changes in the glandular stomach of *Hp*- and cod bone-treated animals were the same as those of *Hp*- and whole cod fish- or 'other parts' diet-treated animals.

In addition to cod bone, sardine bone and prawn shell were administered to *Hp*-infected gerbils. As in the case of cod bone, administration of sardine bone and prawn shell diet did not affect the feeding and body weights in the groups studied. As shown in Table II, the number of animals with edema, the stomach wet weights and the number of hemorrhagic spots per animal were again significantly increased with histological changes in the glandular stomach in these groups similar to those in the cod bone-fed group.

Since most calcium in cod and sardine bones comes from hydroxyapatite and the one in prawn shell is calcium carbonate, calcium-free AIN-76A diet was supplemented with these calcium compounds at 0.22 to 3.50%. Administration of these diets did not affect the feeding or other behavior of the gerbils but effects were noted on *Hp*-induced gastritis (Table III). Among the calcium-administered groups, hydroxyapatite enhanced *Hp*-induced gastritis. The stomach wet weights and the number of hemorrhagic spots per animal were increased significantly by 0.88 and 1.75% doses of hydroxyapatite. However, in the 3.50% hydroxyapatite group, 3 out of five animals were not infected with *Hp* at the end of the experiment, and were free

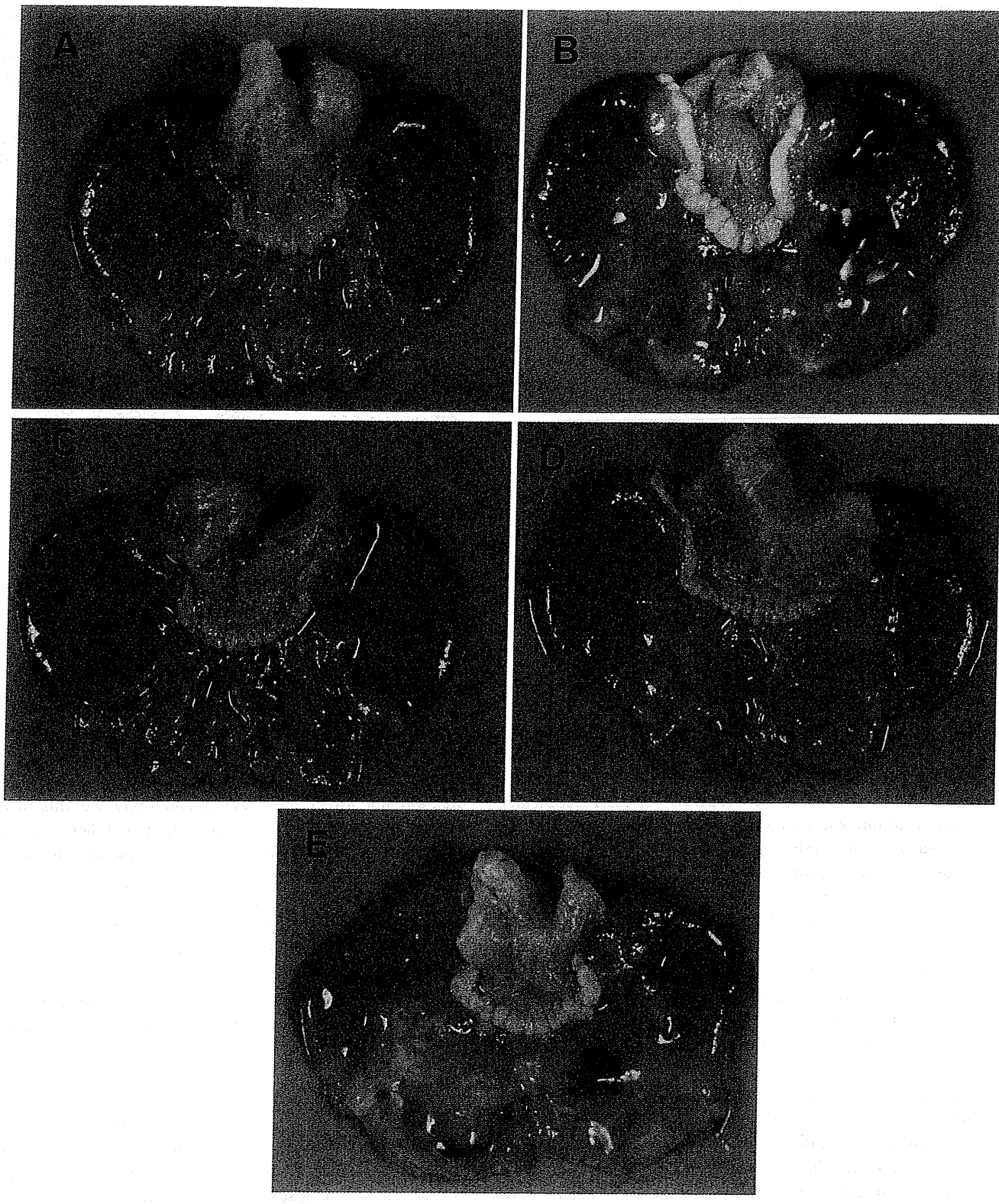

Figure 1. *Typical macroscopic views of glandular stomach of Mongolian gerbils inoculated with Helicobacter pylori (Hp). Treatments: A: 10% Casein basal diet with Hp infection; B: 10% fish meal diet with Hp infection; C: 5.2% meat diet with Hp infection; D: 0.3% viscera diet with Hp infection; E: 4.5% 'other parts' diet with Hp infection.*

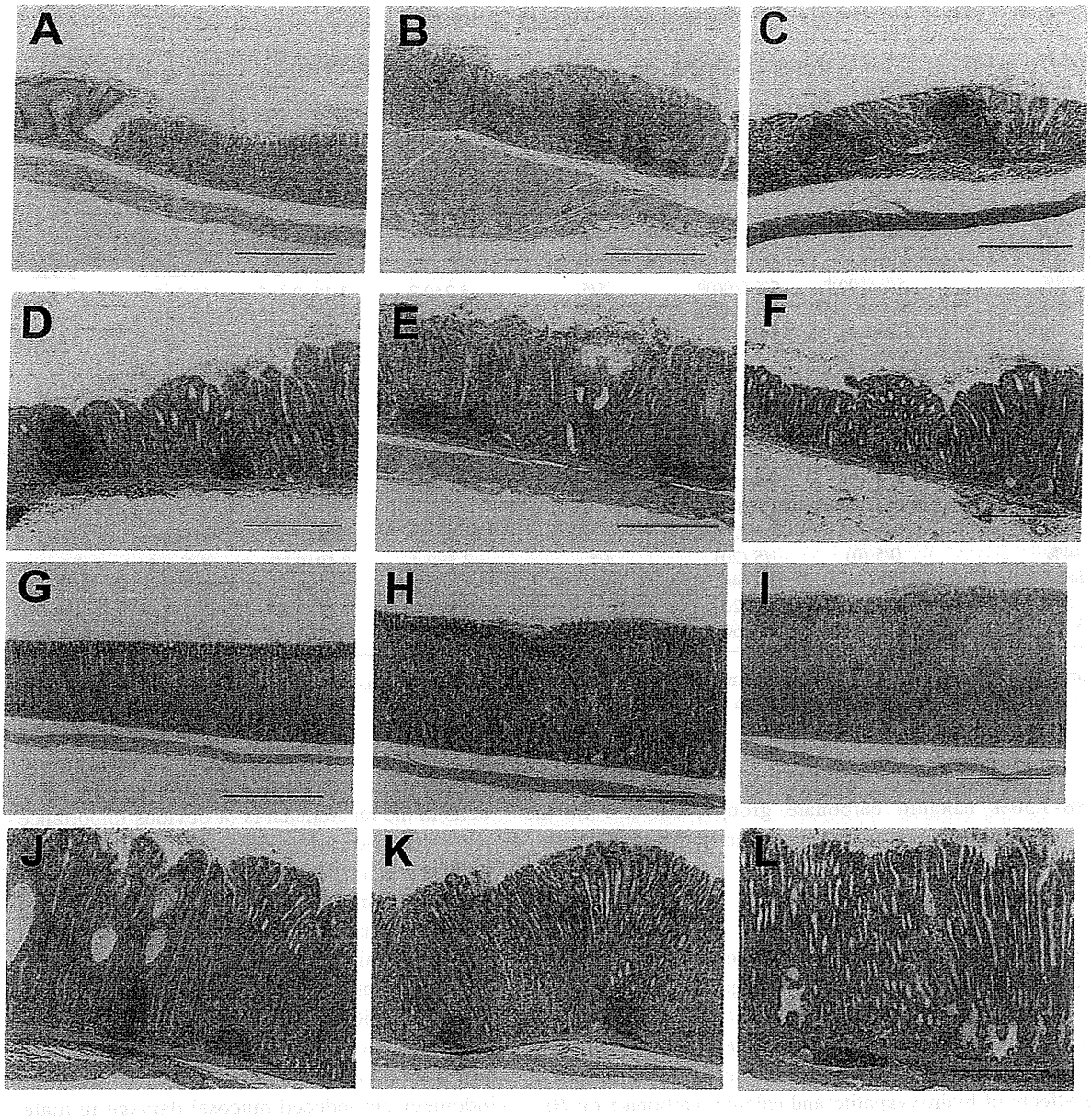

Figure 2. *Typical microscopic views of glandular stomach of Mongolian gerbils without or inoculated with Helicobacter pylori (Hp). Histological findings of sections stained with hematoxylin and eosin of fundic (A-F) and pyloric (G-L) mucosa are presented in the groups treated with 2% cod bone with Hp (C and I), 1.75% hydroxyapatite [$Ca_{10}(PO_4)_6(OH)_2$] with Hp (D and J), 1.75% calcium carbonate ($CaCO_3$) with Hp (E and K), 1.75% calcium hydrogenphosphate dihydrate ($CaHPO_4$) with Hp (F and L). Basal diet groups were inoculated with Hp (B and H) or were without Hp (A and G) and are also shown. Bar=500 μm.*

from gastric hemorrhage, with reduced stomach wet weights. Calcium carbonate had enhancing effects on *Hp*-induced gastritis involving edema and hemorrhage. The stomach wet weights and the number of hemorrhagic spots per animal were increased significantly in the 0.88% calcium carbonate group. However, in the 3.50% calcium carbonate group, stomach wet weights and the numbers of hemorrhagic spots were lower than those in the 0.88% group. In addition, weak, but not statistically significant, enhancing effects on gastritis were observed in the calcium hydrogenphosphate dihydrate groups. Histological changes in the glandular stomach in hydroxyapatite and calcium carbonate groups were similar to those in cod bone- and prawn shell-fed groups, respectively (Figure 2). Serum calcium levels ranged from 9.1-9.9 mg/dl, and were not remarkably changed. Serum gastrin levels were higher in the 1.75% hydroxyapatite and

Table III. *Effects of calcium intake on H. pylori-induced gastritis in Mongolian gerbils.*

Diet	No. of animals (%) with			No. of colonies of *H. pylori* (log CFUs/ stomach)[a]	Stomach wet weight (g)[a]	No. of hemorrhagic spots/animal[a]	Calcium levels in serum (mg/dl)[a]	Gastrin levels in serum (pg/ml)[a]
	Edema	Hemorrhage	*H. pylori* infection					
Basal	0/5 (0)	0/5 (0)	4/5	3.1±0.9	0.67±0.04	0	9.2±0.3	177±6
Hydroxyapatite, $Ca_{10}(PO_4)_6(OH)_2$								
0.22%	3/5 (60)	3/5 (60)	5/5	4.0±0.7	0.89±0.22[e]	4.2±6.7	9.1±0.9	168±78[e]
0.44%	2/5 (40)	1/5 (20)	4/5	4.1±0.5	0.72±0.18	7.0±15.7	9.9±0.2	177±35
0.88%	5/5 (100)[b]	5/5 (100)[b]	5/5	4.2±0.3e	1.19±0.10[d]	12.0±5.4[d]	9.5±0.5	173±32
1.75%	5/5 (100)[b]	5/5 (100)[b]	5/5	4.5±0.3e	1.19±0.13[d]	14.8±5.3[d]	9.4±0.6	277±51[e]
3.50%	0/5 (0)	0/5 (0)	2/5	3.7±0.1	0.53±0.06[d]	0	9.6±0.4	263±31
Calcium carbonate, $CaCO_3$								
0.22%	1/5 (20)	1/5 (20)	5/5	3.9±0.6	0.81±0.17	3.0±6.7	9.4±0.4	170±10
0.44%	2/5 (40)	2/5 (40)	5/5	3.7±0.7	0.88±0.36	6.0±11.3	9.3±0.3	193±32
0.88%	4/5 (80)[c]	4/5 (80)[c]	5/5	4.7±0.7e	0.94±0.23[e]	7.2±7.3[e]	9.4±0.1	227±72[e]
1.75%	3/5 (60)	3/5 (60)	5/5	4.0±0.7	0.86±0.31	12.0±15.6	9.7±0.3	263±105[d]
3.50%	1/5 (20)	1/5 (20)	4/5	4.1±0.4	0.72±0.24	5.2±11.6	9.8±0.6	243±65[e]
Calcium hydrogenphosphate dihydrate, $CaHPO_4 \cdot 2H_2O$								
0.22%	0/5 (0)	1/5 (20)	4/5	3.7±0.5	0.71±0.07	0.2±0.4	9.6±0.3	175±7
0.44%	0/5 (0)	1/5 (20)	4/5	3.6±0.4	0.69±0.07	0.8±1.8	9.8±0.3	180±10
0.88%	1/5 (20)	2/5 (40)	5/5	3.4±1.1	0.77±0.31	6.8±13.6	9.5±0.5	177±25
1.75%	1/5 (20)	1/5 (20)	5/5	3.3±1.2	0.71±0.34	8.4±18.8	9.5±0.2	197±23
3.50%	2/5 (40)	3/5 (60)	5/5	3.7±0.6	0.79±0.31	5.8±8.0	9.8±0.5	193±23

Samples were supplemented to basal (calcium-free AIN-76A) diet. [a]Mean±SD. [b]$p<0.01$ and [c]$p<0.05$ *versus* basal diet group by Fisher's exact test; [d]$p<0.01$ and [e]$p<0.05$ *versus* basal diet group by Welch's *t*-test.

0.88-3.50% calcium carbonate groups, but not in the hydrogenphosphate dihydrate group, as shown in Table III.

Discussion

In the present study, we found that cod bone in fish meal enhanced *Hp*-induced gastritis in Mongolian gerbils and that a similar enhancement was observed with sardine bone and prawn shell administration. To clarify the causative constituents in the fish bones and prawn shell, we examined the effects of hydroxyapatite and calcium carbonate on *Hp*-induced gastritis, and found that both constituents clearly enhanced *Hp*-induced gastritis when fed at 0.22-1.75% in the diet. However, a high dose intake of these compounds (3.5%) resulted in a reduced occurrence of *Hp*-induced gastritis. Calcium hydrogenphosphate dihydrate, included in the AIN-76A diet, also had a weak enhancing effect, but this was not statistically significant.

Several *in vivo* and *in vitro* studies have implied that calcium enhances gastric disorders (16-19). To our knowledge, this is the first report of direct evidence showing that administration of calcium compounds enhances *Hp*-induced gastritis in Mongolian gerbils. Over-secretion of acid (HCl) and loss of feedback control causes gastritis and ulceration. Therefore, the fact that that elevation of extracellular calcium can induce acid secretion from parietal cells in the rat stomach is of obvious importance (16). There are calcium-sensing receptors in G cells and parietal cells, and signals from these receptors play important roles in both acid secretion and mucosal repair (16). Calcium chloride is reported to increase the activity of ornithine decarboxylase and to stimulate DNA synthesis in the pyloric mucosa in F344 male rats (17). In contrast, calcium channel blockers, which inhibit the entry of calcium into cells, attenuate gastritis (18). Calcium channel blockers have been also reported to protect gastric mucosa from ethanol- and indomethacin-induced mucosal damage in male Fisher 344 rats (19). The available data thus suggest that gastritis, gastric ulceration and gastric carcinogenesis might be enhanced by calcium influx. We measured serum calcium levels and gastrin levels as factors responsible for inducing gastric erosion or ulceration by hypergastrinemia and high acid secretion. However, serum calcium levels and gastrin levels did not significantly differ between the gerbils fed basal diet and those fed 10% whole codfish or 'other parts'. Moreover, serum gastrin levels tended to correlate with the amount of hydroxyapatite and calcium carbonate consumption, but not with that of calcium hydrogenphosphate dihydrate. Serum calcium levels and gastrin levels, which may affect gastric pH, may have the same effect on gastritis observed in the present study, but other mechanisms are also suggested to be responsible.

However, epidemiological and experimental studies have demonstrated suppressive effects of calcium intake on gastric cancer development. For example, a case-control study demonstrated gastric cancer risk to be reduced by dietary intake of calcium, carotene, fresh vegetables, fruits and vitamin C (20). One *in vivo* study demonstrated that calcium chloride can inhibit sodium chloride-induced replicative DNA synthesis in the pyloric mucosa of male Fischer 344 rats (21).

In the present study, our data demonstrated enhancing and protective, opposing, effects of calcium on *Hp*-induced gastritis in Mongolian gerbils. The mechanisms involved remain to be clarified. Interestingly, however, calcium may exert inhibitory effects on urease extraction from *Hp*. *Hp* urease is important for facilitating colonization of *Hp* and is correlated with stomach mucosal injury, including gastritis (22-24). Pérez-Pérez *et al*. showed that calcium chloride has little effect on *Hp* urease activity itself, but reduces extraction of urease from *Hp* cells (25). We have reported that urease inhibitors, acetohydroxamic acid and flurofamide, can eradicate *Hp* in Mongolian gerbils (26). These reports allow us to speculate that higher hydroxyapatite- or calcium carbonate-containing diets may eradicate *Hp* in Mongolian gerbils by the inhibition of *Hp* urease extraction.

Daily average intake of calcium by Japanese people from various foods, including fish bone and shrimp shell, is reported to be almost 500 mg per person (27). Thus, the doses of hydroxyapatite and calcium carbonate used in the present study are very much higher than the expected human exposure levels. However, humans continually consume various kinds of foods that may enhance *Hp*-induced gastritis. It is probable that calcium compounds and other dietary factors would have additional or synergistic enhancing effects on *Hp*-induced gastritis. Of note, it is reported that the content of hydroxyapatite-type calcium is around 36% in fish bone (28). This may also be true in the case of the content of calcium carbonate in prawn shell (29). Differences in enhancing effects of *Hp*-induced gastritis among the groups fed diets with hydroxyapatite, calcium carbonate, and calcium hydrogenphosphate dihydrate remain to be elucidated. Moreover, different effects of fishmeal treatment, fish bone treatment and direct calcium treatment on gastric mucosa should be taken into consideration because digestive processes should differ. From the incidence of hemorrhage in each group, direct calcium treatment at doses of 0.88 and 1.75% seem to induce more severe changes than 2% cod bone treatment or treatment with 4.5% 'other parts' diet. These data suggest that calcium itself could be the factor directly affecting functions related to *Hp*-induced gastritis.

The present experimental model may clarify the mechanism of development of peptic ulcer or acute mucosal lesions. This model does not represent chronic inflammation status that usually observed around human gastric cancer tissue because the experimental period is too short to induce chronic inflammation. However, in the *Hp*-infected Mongolian gerbil model with a long experimental period after carcinogen treatment, gastric cancer can be induced with similar pathological changes in humans. Our data may provide basic information for further experiments elucidating the mechanisms of gastric cancer induction.

Since the incidence of gastritis and gastric cancer is high all over the world, it is very important to clarify the effect of calcium on gastritis and to elucidate through further research the detailed mechanisms that enhance gastritis.

Acknowledgements

Authors thank Dr Takayuki Matsumoto, Dr Norihiko Kouyama, Dr Tomoko Mizote, Dr Hideyuki Shibata, Dr Toshihiko Kawamori and Dr Takeji Takamura for their valuable advice and help. We also thank Mr Masanobu Takiguchi for his technical assistance.

References

1 Nomura A: Stomach. *In*: Cancer Epidemiology and Prevention. Schottenfield D and Fraumeni J Jr. (eds.). Philadelphia, WB Saunders, pp. 624-637, 1982.

2 Ernst PB, Peura DA and Crowe SE: The translation of *Helicobacter pylori* basic research to patient care. Gastroenterol *130(1)*: 188-206, 2006.

3 Marshall BJ and Warren JR: Unidentified curved bacilli in the stomach of patients with gastritis and peptic ulceration. Lancet *1(8390)*: 1311-1315, 1984.

4 Parsonnet J, Friedman GD, Vandersteen DP, Vogelman JH, Orentreich N and Sibley RK: *Helicobacter pylori* infection and the risk of gastric carcinoma. N Engl J Med *325(16)*: 1127-1131, 1991.

5 Uemura N, Okamoto S, Yamamoto S, Matsumura N, Yamaguchi S, Yamakido M, Taniyama K, Sasaki N and Schlemper RJ: *Helicobacter pylori* infection and the development of gastric cancer. N Engl J Med *345(11)*: 784-789, 2001.

6 Hirayama F, Takagi S, Yokoyama Y, Iwao E and Ikeda Y: Establishment of gastric *Helicobacter pylori* infection in Mongolian gerbils. J Gastroenterol *31(9)*: 24-28, 1996.

7 Hirayama F, Takagi S, Kusuhara H, Iwao E, Yokoyama Y and Ikeda Y: Induction of gastric ulcer and intestinal metaplasia in Mongolian gerbils infected with *Helicobacter pylori*. J Gastroenterol *31(5)*: 755-757, 1996.

8 Shimizu N, Inada K, Nakanishi H, Tsukamoto T, Ikehara Y, Kaminishi M, Kuramoto S, Sugiyama A, Katsuyama T and Tatematsu M: *Helicobacter pylori* infection enhances glandular stomach carcinogenesis in Mongolian gerbils treated with chemical carcinogens. Carcinogenesis *20(4)*: 669-676, 1999.

9 Sugiyama A, Maruta F, Ikeno T, Ishida K, Kawasaki S, Katsuyama T, Shimizu N and Tatematsu M: *Helicobacter pylori* infection enhances *N*-methyl-*N*-nitrosourea-induced stomach carcinogenesis in the Mongolian gerbil. Cancer Res *58(10)*: 2067-2069, 1998.

10 Tokieda M, Honda S, Fujioka T and Nasu M: Effect of *Helicobacter pylori* infection on the *N*-methyl-*N'*-nitro-*N*-nitrosoguanidine-induced gastric carcinogenesis in mongolian gerbils. Carcinogenesis *20(7)*: 1261-1266, 1999.

11 Kato S, Tsukamoto T, Mizoshita T, Tanaka H, Kumagai T, Ota H, Katsuyama T, Asaka M and Tatematsu M: High salt diets dose-dependently promote gastric chemical carcinogenesis in *Helicobacter pylori*-infected Mongolian gerbils associated with a shift in mucin production from glandular to surface mucous cells. Int J Cancer *119(7)*: 1558-1566, 2006.

12 Matsubara S, Takasu S, Tsukamoto T, Mutoh M, Masuda S, Sugimura T, Wakabayashi K and Totsuka Y: Induction of glandular stomach cancers in *Helicobacter pylori*-infected Mongolian gerbils by 1-nitrosoindole-3-acetonitrile. Int J Cancer *130(2)*: 259-266, 2012.

13 Tanigawa T, Kawamori T, Iimuro M, Ohta T, Higuchi K, Arakawa T, Sugimura T and Wakabayashi K: Marked enhancement by fish meal of *Helicobacter pylori*-induced gastritis in Mongolian gerbils. Jpn J Cancer Res *91(8)*: 769-773, 2000.

14 Blaser MJ: Hypothesis: The changing relationships of *Helicobacter pylori* and humans: Implications for health and disease. J Infect Dis *181(2)*: 805-806, 2000.

15 International Agency for Research on Cancer: Schistosomes, Liver Flukes and *Helicobacter pylori*. *In*: IARC Monogr Eval Carcinog Risks Hum 61. Lyon, IARC, pp. 177-240, 1994.

16 Kirchhoff P and Geibel JP: Role of calcium and other trace elements in the gastrointestinal physiology. World J Gastroenterol *12(20)*: 3229-3236, 2006.

17 Furihata C, Yamakoshi A, Takezawa R and Matsushima T: Various sodium salts, potassium salts, a calcium salt and an ammonium salt induced ornithine decarboxylase and stimulated DNA synthesis in rat stomach mucosa. Jpn J Cancer Res *80(5)*: 424-429, 1989.

18 Tatsuta M, Iishi H, Baba M, Nakaizumi A, Uehara H and Taniguchi H: Effect of calcium channel blockers on gastric carcinogenesis and caerulein enhancement of gastric carcinogenesis induced by *N*-methyl-*N*'-nitro-*N*-nitrosoguanidine in Wistar rats. Cancer Res *50(7)*: 2095-2098, 1990.

19 Ghanayem BI, Matthews HB and Maronpot RR: Calcium channel blockers protect against ethanol- and indomethacin-induced gastric lesions in rats. Gastroenterology *92(1)*: 106-111, 1987.

20 You WC, Blot WJ, Chang YS, Ershow AG, Yang ZT, An Q, Henderson B, Xu GW, Fraumeni JF Jr. and Wang TG: Diet and high risk of stomach cancer in Shandong, China. Cancer Res *48(12)*: 3518-3523, 1988.

21 Furihata C, Sudo K and Matsushima T: Calcium chloride inhibits stimulation of replicative DNA synthesis by sodium chloride in the pyloric mucosa of rat stomach. Carcinogenesis *10(11)*: 2135-2137, 1989.

22 Eaton KA, Brooks CL, Morgan DR and Krakowka S: Essential role of urease in pathogenesis of gastritis induced by *Helicobacter pylori* in gnotobiotic piglets. Infect Immun *59(7)*: 2470-2475, 1991.

23 Chen XG, Correa P, Offerhaus J, Rodriguez E, Janney F, Hoffmann E, Fox J, Hunter F and Diavolitsis S: Ultrastructure of the gastric mucosa harboring *Campylobacter*-like organisms. Am J Clin Pathol *86(5)*: 575-582, 1986.

24 Hazell SL, Lee A, Hazell SL and Lee A: *Campylobacter pyloridis*, urease, hydrogen ion back diffusion, and gastric ulcers. Lancet *2(8497)*: 15-17, 1986.

25 Pérez-Pérez GI, Gower CB and Blaser MJ: Effects of cations on *Helicobacter pylori* urease activity, release, and stability. Infect Immun *62(1)*: 299-302, 1994.

26 Ohta T, Shibata H, Kawamori T, Iimuro M, Sugimura T and Wakabayashi K: Marked reduction of *Helicobacter pylori*-induced gastritis by urease inhibitors, acetohydroxamic acid and flurofamide, in Mongolian gerbils. Biochem Biophys Res Commun *285(3)*: 728-733, 2001.

27 National Health and Nutrition Survey 2009. *In*: Ministry of Health, Labour and Welfare Japan, 2009. Available at: http://www.mhlw.go.jp/bunya/kenkou/eiyou/dl/h21-houkoku-01.pdf

28 Hamada M, Nagai T, Kai N, Tanoue Y, Mae H, Hashimoto M, Miyoshi K, Kumagai H and Saeki K: Inorganic constituents of bone of fish. Fisheries Sci *61(3)*: 517-520,1995.

29 Xu Y, Gallert C and Winter J: Chitin purification from shrimp wastes by microbial deproteination and decalcification. Appl Microbiol Biotechnol *79*: 687-697, 2008.

Received July 8, 2013
Revised July 26, 2013
Accepted July 29, 2013

Ann Nucl Med (2013) 27:640–647
DOI 10.1007/s12149-013-0729-1

ORIGINAL ARTICLE

SPECT/CT of lung nodules using ^{111}In-DOTA-c(RGDfK) in a mouse lung carcinogenesis model

Takuya Hayakawa · Michihiro Mutoh · Toshio Imai · Koji Tsuta · Akinori Yanaka · Hirofumi Fujii · Mitsuyoshi Yoshimoto

Received: 16 October 2012 / Accepted: 10 April 2013 / Published online: 23 April 2013

Abstract
Objective Lung cancer is one of the leading causes of cancer-related deaths worldwide, including Japan. Although computed tomography (CT) can detect small lung lesions such as those appearing as ground glass opacity, it cannot differentiate between malignant and non-malignant lesions. Previously, we have shown that single photon emission computed tomography (SPECT) imaging using ^{111}In-1,4,7,10-tetraazacyclododecane-*N*,*N*′,*N*″,*N*‴-tetraacetic acid-cyclo-(Arg-Gly-Asp-D-Phe-Lys) (DOTA-c(RGDfK)), an imaging probe of $\alpha_v\beta_3$ integrin, is useful for the early detection of pancreatic cancer in a hamster pancreatic carcinogenesis model. In this study, we aimed to assess the usefulness of SPECT/CT with ^{111}In-DOTA-c(RGDfK) for the evaluation of the malignancy of lung cancer.
Methods Lung tumors were induced by a single intraperitoneal injection (250 mg/kg) of urethane in male A/J mice. Twenty-six weeks after the urethane treatment, SPECT was performed an hour after injection of ^{111}In-DOTA-c(RGDfK). Following this, the radioactivity ratios of tumor to normal lung tissue were measured by autoradiography (ARG) in the excised lung samples. We also examined the expression of $\alpha_v\beta_3$ integrin in mouse and human lung samples.
Results Urethane treatment induced 5 hyperplasias, 41 adenomas and 12 adenocarcinomas in the lungs of 8 A/J mice. SPECT with ^{111}In-DOTA-c(RGDfK) could clearly visualize lung nodules, though we failed to detect small lung nodules like adenoma and hyperplasias (adenocarcinoma: 66.7 %, adenoma: 33.6 %, hyperplasia: 0.0 %). ARG analysis revealed significant uptake of ^{111}In-DOTA-c(RGDfK) in all the lesions. Moreover, tumor to normal lung tissue ratios increased along with the progression of carcinogenesis. Histopathological examination using human lung tissue samples revealed clear up-regulation of $\alpha_v\beta_3$ integrin in well-differentiated adenocarcinoma (Noguchi type B and C) rather than atypical adenomatous hyperplasia.
Conclusion Although there are some limitations in evaluating the malignancy of small lung tumors using ^{111}In-DOTA-c(RGDfK), SPECT with ^{111}In-DOTA-c(RGDfK) might be a useful non-invasive imaging approach for evaluating the characteristics of lung tumors in mice, thus showing potential for use in humans.

Keywords ^{111}In-DOTA-c(RGDfK) · SPECT · Carcinogenesis · Lung cancer

T. Hayakawa · M. Mutoh
Division of Cancer Prevention Research, National Cancer Center Research Institute, 5-1-1 Chuo-ku, Tokyo 104-0045, Japan

T. Hayakawa · A. Yanaka
Faculty of Pharmaceutical Sciences, Tokyo University of Science, 2641 Yamazaki, Noda, Chiba 278-8510, Japan

T. Imai
Central Animal Division, National Cancer Center Research Institute, 5-1-1 Chuo-ku, Tokyo 104-0045, Japan

K. Tsuta
Division of Pathology and Clinical Laboratory, National Cancer Center Hospital, 5-1-1 Chuo-ku, Tokyo 104-0045, Japan

H. Fujii · M. Yoshimoto
Functional Imaging Division, National Cancer Center Hospital East, 6-5-1 Kashiwanoha, Kashiwa, Chiba 277-8577, Japan

M. Yoshimoto (✉)
Division of Cancer Development System, National Cancer Center Research Institute, 5-1-1 Tsukiji, Chuo-ku, Tokyo 104-0045, Japan
e-mail: miyoshim@ncc.go.jp

algorithm on dedicated software (Invivoscope; Bioscan, Inc., Washington, DC, USA) and Mediso InterViewXP (Mediso, Budapest, Hungary). SPECT and CT images were automatically superimposed by Invivoscope. The accuracy of superimposition was calibrated at regular intervals using phantoms. A researcher experienced in the evaluation of small animal SPECT/CT images visually judged pulmonary uptake.

Autoradiography with ^{111}In-DOTA-c(RGDfK) in the mouse lung carcinogenesis model

After SPECT/CT imaging, the lungs were excised and macroscopically surveyed to detect lung tumor lesions. Samples were then embedded in Cryo Mount II (Muto Pure Chemicals Co., Ltd., Tokyo, Japan) and frozen in liquid nitrogen. Frozen sections were mounted on glass slides after being cut with a cryostat into 20-μm thick sections for autoradiography (ARG) and 10-μm thick sections for histological analysis. The glass slides were then placed on an imaging plate (BAS-MS 2040; Fuji film Co., Ltd., Tokyo, Japan). Radioactivity was detected by scanning with a bioimaging analyzer (FLA-7000, Fuji film Co., Ltd., Tokyo, Japan). Based on the microscopic observation of hematoxylin and eosin (H&E) stained sections, regions of interest were placed on both tumor and normal lung regions. Image Quant software (Multi gauge, Fuji film Co., Ltd., Tokyo, Japan) was used to quantify the intensity of radioactivity.

Human lung tissue microarray (TMA)

The expression of $\alpha_v\beta_3$ integrin in various types of human lung lesions was tested using TMA. A total of 48 tissue samples were embedded in TMA sections, including bronchial tubes, normal lung tissue, adenocarcinoma (poorly, moderately, and well differentiated), squamous cell carcinoma, large cell neuroendocrine carcinoma, and mesothelioma. The study protocol was approved by the institutional review board of the NCC, Tokyo, Japan.

Human lung tissue samples

A total of 34 lung tissue samples were obtained from patients who underwent lobectomies at the National Cancer Center (NCC) Hospital from 2006 to 2008. The paraffin-embedded sample stocks were immunohistochemically stained for $\alpha_v\beta_3$ integrin. The samples included atypical adenomatous hyperplasia (AAH, $n = 16$), localized bronchioloalveolar carcinoma with alveolar collapse (Noguchi type B, $n = 11$), and localized bronchioloalveolar carcinoma with foci of active fibroblastic proliferation (Noguchi type C, $n = 10$), which could be classified as GGOs on clinical CT images. The study protocol was approved by the institutional review board of the NCC, Tokyo, Japan.

Immunohistochemistry for $\alpha_v\beta_3$ integrin

The excised mice and human lung sections were used for immunohistochemical examination using the avidin–biotin complex immunoperoxidase technique. Sections were incubated with anti-$\alpha_v\beta_3$ integrin (clone LM609; Millipore, Billerica, MA, USA) overnight at 4 °C. Sections were incubated with biotinylated anti-mouse IgG (Dako Cytomation, Glostrup, Denmark), followed by reaction with streptavidin–biotin horseradish peroxidase (HRP) complex (Strept ABComplex/HRP; Dako Cytomation). HRP was detected by 3,3′-diaminobenzidine (Phoenix Biotechnologies, Huntsville, AL, USA) substrate. All sections were counterstained with hematoxylin.

Evaluation of staining intensity

Sections were evaluated randomly without knowledge of patient history. Each specimen wherein more than 10 % of the cancer cells reacted positively for an antibody were recorded as positive. The sections were classified according to staining intensity as negative (total absence of staining), 1+ (weak staining), 2+ (moderate staining), or 3+ (strong staining).

Statistical analysis

Statistical analysis was performed using JMP IN version 5 statistical software (SAS Institute, Cary, NC, USA). Mann–Whitney test was employed to numerical data that did not show a normal distribution (comparison of T/N ratio). χ^2 tests were applied to compare the difference in the detection rate using SPECT in different tumor stage. Values are reported as mean ± SD. A two-tailed p value of <0.05 was considered statistically significant.

Results

SPECT with ^{111}In-DOTA-c(RGDfK) in the urethane-treated mice

In total, 58 lung lesions were macroscopically found in the 8 urethane-treated mice. Of the 58 lesions, 12 were adenocarcinomas (average size, 1.87 ± 0.58 mm), 41 were adenomas (average size, 1.45 ± 0.31 mm), and 5 were hyperplasias (average size, 1.34 ± 0.42 mm). As shown in Table 1, SPECT with ^{111}In-DOTA-c(RGDfK) detected 8 adenocarcinomas (66.7 %), 15 adenomas (36.6 %), and 0 hyperplasias (0.0 %). These detection rates were

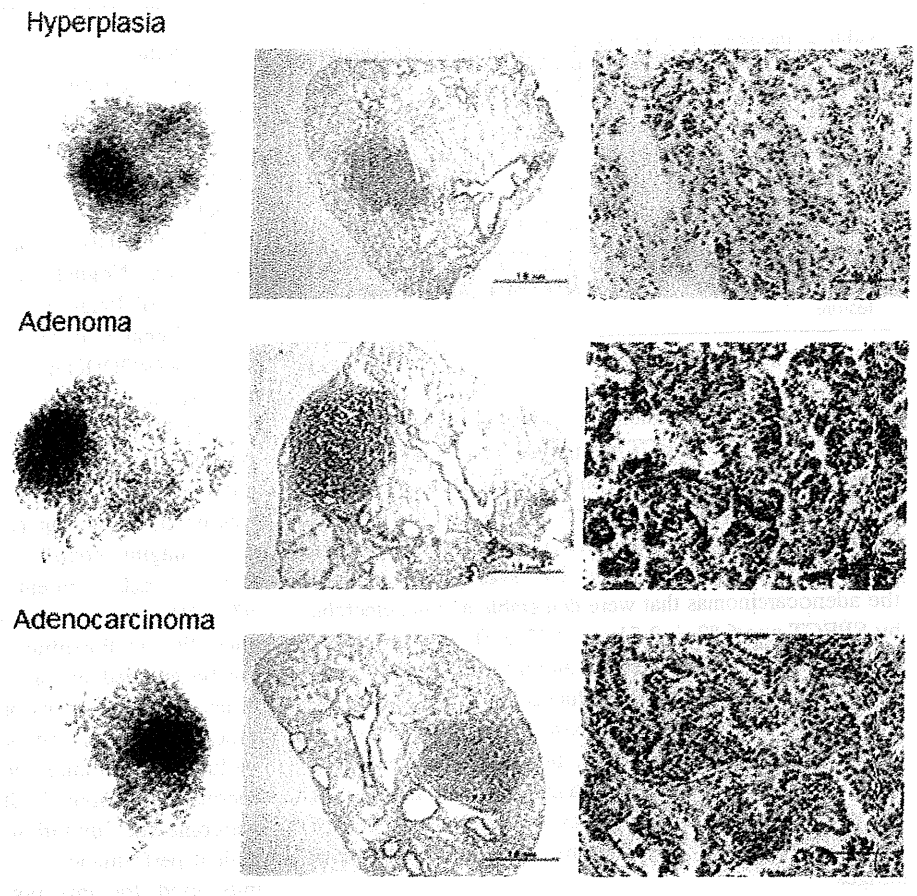

Fig. 2 Ex vivo autoradiography and H&E staining of representative lung sections. Strong hot spots were found in the right upper lobes by ARG (*left lane*). H&E staining of lung sections (*middle lane*) and high magnification of lung lesions (*right lane*)

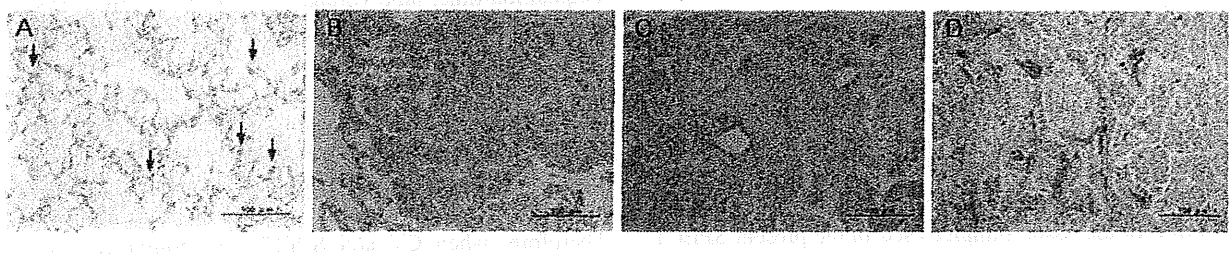

Fig. 3 $\alpha_v\beta_3$ integrin expression in the lung lesions of A/J mice. **a** Normal lung tissue. Type II pneumocytes expressing negligible levels of $\alpha_v\beta_3$ integrin (*arrow*). **b** Hyperplasia, **c** adenoma, and **d** adenocarcinoma

of $\alpha_v\beta_3$ integrin was observed in type II pneumocyte and Clara cells (Figs. 3a and 4c). Consistent with this observation, ^{111}In-DOTA-c(RGDfK) was accumulated in bronchial tubes of the A/J mice (Fig. 4a).

Expression of $\alpha_v\beta_3$ integrin in various types of human lung tumors

Expression of $\alpha_v\beta_3$ integrin was evaluated using TMA including several tissue types such as adenocarcinoma, squamous cell carcinoma, large cell neuroendocrine carcinoma, and mesothelioma. Among them, strong and extensive immunoreactivity for $\alpha_v\beta_3$ integrin was found in differentiated tubular adenocarcinoma.

We further examined staining intensity of $\alpha_v\beta_3$ integrin in AAH, Noguchi type B and Noguchi type C lesions (Fig. 5), and the incidence of positive cases is summarized in Table 2. The incidence of $\alpha_v\beta_3$ integrin-positivity was high for Noguchi type B (91 %) and Noguchi type C (90 %). In contrast, relatively lower expression (63 %) was observed in AAH lesions.

Staining intensity correlated with tumor aggressiveness. The incidence of strong positivity (+++) among the AAH, Noguchi type B, and Noguchi type C lesions was 6.3, 27.3,

Table 2 Incidence of $\alpha_v\beta_3$ integrin expression in human lung lesions

$\alpha_v\beta_3$ Intensity	AAH (%)	Noguchi type B (%)	Noguchi type C (%)
−	6/16 (37.5)	1/11 (9.1)	1/10 (10.0)
+	3/16 (18.8)	1/11 (9.1)	1/10 (10.0)
++	6/16 (37.5)	6/11 (54.5)	3/10 (30.0)
+++	1/16 (6.3)	3/11 (27.3)	5/10 (50.0)
Total positive lesions	10/16 (62.5)	10/11 (90.9)	9/10 (90)

Therefore, a low detection rate may be explained by the limitations of the SPECT technique itself with regard to small lesion size and/or low uptake in the lesions. In fact, the average size of the adenocarcinomas that were detectable and undetectable by SPECT was 2.09 ± 0.59 and 1.43 ± 0.17 mm, respectively. The average T/N ratio of the adenocarcinomas that were detectable and undetectable by SPECT was 6.82 ± 2.51 and 4.27 ± 0.53, respectively. Therefore, the size of the tumor and the uptake of tracer by the tumor have significant influence on SPECT images. The low detection rate may also be explained by the deterioration of SPECT images. Because of movement of the heart and the thoracic diaphragm, lesions in the hilus of the lung or at the periphery may be overlooked because cardiac motion may prevent the visualization of clear images.

SPECT with ^{111}In-DOTA-c(RGDfK) seems to be useful in the detection of malignant lesions because the T/N ratio of adenocarcinoma is significantly greater than that of hyperplasia ($p < 0.05$). Moreover, in accordance with the increase of the T/N ratio, the detection rate by SPECT was highest in adenocarcinomas. We could not show the relationship between the uptake of ^{111}In-DOTA-c(RGDfK) and the $\alpha_v\beta_3$ integrin expression level in this study because the condition of the tissue samples used in the present SPECT study was poor for the immunohistochemical semi-quantitative analysis. However, it has already been reported that the accumulation level of RGD peptide probe correlates with the expression level of $\alpha_v\beta_3$ integrin [16]. Thus, it is thought that the difference of accumulation level of ^{111}In-DOTA-c(RGDfK) between adenocarcinoma, adenoma, and hyperplasia in our present study is also reflecting the expression level of $\alpha_v\beta_3$ integrin.

The role of the $\alpha_v\beta_3$ integrin in lung cancer is unclear. However, the $\alpha_v\beta_3$ expression in breast cancer, pancreatic cancer, and prostate cancer contributes to tumor progression and metastasis [17–19]. High uptake of ^{111}In-DOTA-c(RGDfK) by lung cancer lesions might estimate metastatic potential to spread to the brain and bones.

We recently reported that ^{111}In-DOTA-c(RGDfK) is superior to 2-deoxy-2-[^{18}F]fluoro-D-glucose in the differentiation of inflammatory lesions [13]. It is highly effective in identifying malignant lesions that appear as GGOs. During histopathological examination of human lung tissue samples, we observed a high incidence and the strong expression of $\alpha_v\beta_3$ integrin in Noguchi type B and Noguchi type C lesions. These results suggested that ^{111}In-DOTA-c(RGDfK) would preferentially identify Noguchi type B and Noguchi type C. At present, there are no other methods of long-term follow-up for the determination of the malignancy of GGOs. SPECT/CT imaging with ^{111}In-DOTA-c(RGDfK) may help in determining whether biopsy to arrive at a definitive diagnosis should be performed.

Our histopathological examination also revealed that type II pneumocytes express low levels of $\alpha_v\beta_3$ integrin. Although $\alpha_v\beta_3$ integrin expression in type II pneumocytes was negligible in our study, it did not appear to interfere with imaging contrast. We also found that Clara cells express $\alpha_v\beta_3$ integrin. Furthermore, ^{111}In-DOTA-c(RGDfK) accumulated in the bronchial tubes of the A/J mice (Fig. 1). Potentially, this type of false positive finding can be avoided by procuring CT images because reconstructed three-dimensional images easily differentiate tumors (globular) and bronchial tubes (tube structure) in the lungs, even though both have similar X-ray absorption. Therefore, combined SPECT/CT has the potential to overcome the limitations of SPECT alone. Because the clinical performance of CT scanners is better than that of units used for imaging small animals with regard to acquisition time, tube voltage, and current × time product (mAs), identification of the lung structure would be easier in clinical practice.

Furthermore, in our animal experiments, breathing motion affected the degradation of SPECT images because of the long acquisition time. Respiratory-gating systems are now available in clinical SPECT/CT scanners, and this is aiding in the procurement of much more accurate images. Therefore, when CT and SPECT are combined, clearer images can be obtained in clinical practice.

Recently, clinical examinations using ^{99m}Tc-3PRGD for imaging of lung cancer have reported that ^{99m}Tc-3PRGD imaging has sensitivity for the detection of lung malignancies, though the specificity is low [20, 21]. Our study using a carcinogenesis animal model and human tissue samples has provided helpful information that can aid in the diagnosis of lung tumors using radiolabeled RGD.

Conclusion

The present study demonstrated that there are some limitation in detecting mouse lung tumors by SPECT/CT imaging using ^{111}In-DOTA-c(RGDfK), but ^{111}In-DOTA-c(RGDfK) has a possibility to evaluate the malignancy of

lung tumor. In addition, histopathological analysis using human lung tissue samples revealed a high incidence of $\alpha_v\beta_3$ integrin expression in Noguchi type B and Noguchi type C lesions. We therefore believe that ^{111}In-DOTA-c(RGDfK) and other $\alpha_v\beta_3$ integrin imaging agents may be effective in evaluating the malignant potential of lung lesions appearing as GGOs.

Acknowledgments This work was supported in part by a Grant-in-Aid for Exploratory Research and a Grant-in-Aid for Young Scientists (B) from the Ministry of Education, Culture, Sports, Science, and Technology as well as Grants-in-Aid for Cancer Research and for the Third-Term Comprehensive 10-Year Strategy for Cancer Control from the Ministry of Health, Labour and Welfare of Japan. The authors would like to thank Enago (http://www.enago.jp) for the English language review.

Conflict of interest The authors have no conflicts of interest to declare.

References

1. Jemal A, Thun MJ, Ries LA, Howe HL, Weir HK, Center MM, et al. Annual report to the nation on the status of cancer, 1975–2005, featuring trends in lung cancer, tobacco use, and tobacco control. J Natl Cancer Inst. 2008;100:1672–94.
2. Aberle DR, Adams AM, Berg CD, Black WC, Clapp JD, Fagerstrom RM, et al. Reduced lung-cancer mortality with low-dose computed tomographic screening. N Engl J Med. 2011;365:395–409.
3. MacMahon H, Austin JH, Gamsu G, Herold CJ, Jett JR, Naidich DP, et al. Guidelines for management of small pulmonary nodules detected on CT scans: a statement from the Fleischner Society. Radiology. 2005;237:395–400.
4. Hori Y, Takasuka N, Mutoh M, Kitahashi T, Kojima S, Imaida K, et al. Periodic analysis of urethane-induced pulmonary tumors in living A/J mice by respiration-gated X-ray microcomputed tomography. Cancer Sci. 2008;99:1774–7.
5. Brooks PC. Role of integrins in angiogenesis. Eur J Cancer. 1996;32A:2423–9.
6. Brooks PC, Clark RA, Cheresh DA. Requirement of vascular integrin $\alpha_v\beta_3$ for angiogenesis. Science. 1994;264:569–71.
7. Mizejewski GJ. Role of integrins in cancer: survey of expression patterns. Proc Soc Exp Biol Med. 1999;222:124–38.
8. Albert JM, Cao C, Geng L, Leavitt L, Hallahan DE, Lu B. Integrin $\alpha_v\beta_3$ antagonist cilengitide enhances efficacy of radiotherapy in endothelial cell and non-small-cell lung cancer models. Int J Radiat Oncol Biol Phys. 2006;65:1536–43.
9. Beer AJ, Schwaiger M. Imaging of integrin $\alpha_v\beta_3$ expression. Cancer Metastasis Rev. 2008;27:631–44.
10. Haubner R, Weber WA, Beer AJ, Vabuliene E, Reim D, Sarbia M, et al. Noninvasive visualization of the activated $\alpha_v\beta_3$ integrin in cancer patients by positron emission tomography and [^{18}F]Galacto-RGD. PLoS Med. 2005;2:e70.
11. Haubner R, Wester HJ, Weber WA, Mang C, Ziegler SI, Goodman SL, et al. Noninvasive imaging of $\alpha_v\beta_3$ integrin expression using ^{18}F-labeled RGD-containing glycopeptide and positron emission tomography. Cancer Res. 2001;61:1781–5.
12. Yoshimoto M, Ogawa K, Washiyama K, Shikano N, Mori H, Amano R, et al. $\alpha_v\beta_3$ Integrin-targeting radionuclide therapy and imaging with monomeric RGD peptide. Int J Cancer. 2008;123:709–15.
13. Yoshimoto M, Hayakawa T, Mutoh M, Imai T, Tsuda K, Kimura S, et al. In vivo SPECT Imaging with ^{111}In-DOTA-c(RGDfK) to detect early pancreatic cancer in a hamster pancreatic carcinogenesis model. J Nucl Med. 2012;53:765–71.
14. Festing MF, Lin L, Devereux TR, Gao F, Yang A, Anna CH, et al. At least four loci and gender are associated with susceptibility to the chemical induction of lung adenomas in A/J × BALB/c mice. Genomics. 1998;53:129–36.
15. Gariboldi M, Manenti G, Canzian F, Falvella FS, Radice MT, Pierotti MA, et al. A major susceptibility locus to murine lung carcinogenesis maps on chromosome 6. Nat Genet. 1993;3:132–6.
16. Jin ZH, Furukawa T, Galibert M, Boturyn D, Coll JL, Fukumura T, et al. Noninvasive visualization and quantification of tumor $\alpha_v\beta_3$ integrin expression using a novel positron emission tomography probe, ^{64}Cu-cyclam-RAFT-c(-RGDfK-)$_4$. Nucl Med Biol. 2011;38:529–40.
17. Sloan EK, Pouliot N, Stanley KL, Chia J, Moseley JM, Hards DK, et al. Tumor-specific expression of $\alpha_v\beta_3$ integrin promotes spontaneous metastasis of breast cancer to bone. Breast Cancer Res. 2006;8:R20.
18. McCabe NP, De S, Vasanji A, Brainard J, Byzova TV. Prostate cancer specific integrin $\alpha_v\beta_3$ modulates bone metastatic growth and tissue remodeling. Oncogene. 2007;26:6238–43.
19. Hosotani R, Kawaguchi M, Masui T, Koshiba T, Ida J, Fujimoto K, et al. Expression of integrin $\alpha_v\beta_3$ in pancreatic carcinoma: relation to MMP-2 activation and lymph node metastasis. Pancreas. 2002;25:e30–5.
20. Ma Q, Ji B, Jia B, Gao S, Ji T, Wang X, et al. Differential diagnosis of solitary pulmonary nodules using ^{99m}Tc-3P$_4$-RGD$_2$ scintigraphy. Eur J Nucl Med Mol Imaging. 2011;38:2145–52.
21. Zhu Z, Miao W, Li Q, Dai H, Ma Q, Wang F, et al. ^{99m}Tc-3PRGD2 for integrin receptor imaging of lung cancer: a multicenter study. J Nucl Med. 2012;53:716–22.